Communications Earth & Environment

Article in Press

https://doi.org/10.1038/s43247-026-03710-w

Carbon dioxide removals by tropical moist forests offset most land-use emissions across 18 Afrotropical countries

Received: 7 January 2026

Accepted: 28 May 2026

Cite this article as: Verbiest, W.W., Bauters, M., Lewis, S.L. *et al.* Carbon dioxide removals by tropical moist forests offset most land-use emissions across 18 Afrotropical countries. *Commun Earth Environ* (2026). https://doi.org/10.1038/s43247-026-03710-w

William W. M. Verbiest, Marijn Bauters, Simon L. Lewis, Félicien Meunier, Luke T. Smallman, Philippe Ciais, Jean-François Bastin, Pierre Regnier, Adeline Fayolle, Anaïs Gorel, Jean-Remy Makana, Corneille E. N. Ewango, Auke van der Woude, Liang Feng, Fei Jiang, Paul I. Palmer, Ingrid T. Luijkx, Bhely Angoboy Ilondea, Alfred Ngomanda, Benjamin Toirambe, Yu Feng & Wannes Hubau

Carbon dioxide removals by tropical moist forests offset most land-use emissions across 18 Afrotropical countries

Authors: William W.M. Verbiest[1,2,3*], Marijn Bauters[2], Simon L. Lewis[4,5], Félicien Meunier[2,6], T. Luke Smallman[7], Philippe Ciais[8], Jean-François Bastin[9], Pierre Regnier[10], Adeline Fayolle[9,11], Anaïs Gorel[9], Jean-Remy Makana[12], Corneille E. N. Ewango[13], Auke van der Woude[14], Liang Feng[7], Fei Jiang[15], Paul I. Palmer[7], Ingrid T. Luijkx[14], Bhely Angoboy Ilondea[16], Alfred Ngomanda[17], Benjamin Toirambe[3,18], Yu Feng[8,19], Wannes Hubau[1,3]

Affiliations:

1. Department of Environment, Laboratory of Wood Technology (Woodlab), Ghent University, Ghent, Belgium.

2. Department of Environment, Q-ForestLab, Ghent University, Ghent, Belgium.

3. Service of Wood Biology, Royal Museum for Central Africa, Tervuren, Belgium.

4. School of Geography, University of Leeds, Leeds, United Kingdom.

5. Department of Geography, University College London, London, United Kingdom.

6. Department of water and climate, Vrije Universiteit Brussel, Brussels, Belgium.

7. School of GeoSciences and National Centre for Earth Observation, University of Edinburgh, Edinburgh, EH9 3FF, United Kingdom.

8. Laboratoire des Sciences du Climat et de l'Environnement, CEA-CNRS-UVSQ, Gif-sur-Yvette 91190, France.

9. TERRA Teaching and Research Centre (Forest is Life), Gembloux Agro-Bio Tech, University of Liege, Passage des Déportés n°2, 5030 Gembloux, Belgium.

10. Department of Geoscience, Environment & Society (DGES)-BGEOSYS, Université Libre de Bruxelles, 1050, Brussels, Belgium.

11. CIRAD, Forest and Societies research unit, Montpellier, France.

12. Faculté des Sciences, Laboratoire d'Écologie et Aménagement Forestier, Université de Kisangani, Kisangani, Democratic Republic of Congo.

13. Faculté de Gestion de Ressources Naturelles Renouvelables, Université de Kisangani, Kisangani, Democratic Republic of Congo.

14. Environmental Sciences Group, Wageningen University, Wageningen, The Netherlands.

15. International Institute for Earth System Science Nanjing University, Nanjing, China

16. Institut National pour l'Études et la Recherche Agronomiques, Avenue des Cliniques 13, Kinshasa, RD Congo.

17. Centre National de la Recherche Scientifique et Technologique (CENAREST), Libreville, Gabon.

18. Ministère de l'Environnement et Développement Durable, Kinshasa, Democratic Republic of the Congo.

19. Ningbo Institute of Digital Twin, Eastern Institute of Technology, Ningbo, China.

* Corresponding author: william.verbiest@ugent.be

ORCID accounts:

W.W.M.V.: 0000-0002-0548-6455

C.E.N.E.: 0000-0001-5622-5127

J.-R.M.: 0000-0002-6006-2938

B.A.I.: 0000-0001-9333-8964

M.B.: 0000-0003-0978-6639

A.F.: 0000-0002-6770-0031

A.G.: 0000-0003-0768-5615

T.L.S.: 0000-0002-0835-1003

F.M.: 0000-0003-2486-309X

P.R.: 0000-0002-4531-0868

P.C.: 0000-0001-8560-4943

S.L.: 0000-0002-8066-6851

Y.F.: 0000-0001-6433-5035

F.J.: 0000-0003-1744-7565

P.I.P.: 0000-0002-1487-0969

L.F.: /

I.L.: 0000-0002-3990-6737

A.W.: 0000-0002-6286-2621

A.N.: 0000-0003-2294-905X

B.T.: /

W.H.: 0000-0003-3795-4986

Abstract

African tropical moist forests are critical regulators of global carbon cycling, yet their contributions to national carbon budgets remain poorly constrained, impairing effective policy design. Here, we unravel carbon removals and emissions for 18 African tropical countries using multiple approaches over a data-rich period (2015-2019). Across countries, carbon removals (-286±68.4 TgC yr^{-1}) nearly offset land-use change emissions (343.4±100.3 TgC yr^{-1}), with consistent net fluxes between bottom-up and top-down approaches (57.4±121.4 TgC yr^{-1} versus 99.4±164.5 TgC yr^{-1}). Results vary between countries, with highest removals in intact forests in the Democratic Republic of the Congo (-81.7±64.2 TgC yr^{-1}), lowest land-use change emissions in Gabon (2.6±7.1 TgC yr^{-1}), and highest fossil fuel emissions in Nigeria (31.2±1.6 TgC yr^{-1}). African tropical countries show high carbon removal rates and land-use change emissions but low fossil fuel emissions, contrasting with industrialized countries. (Inter)nationally endorsed conservation policies can reverse national carbon budgets from net sources to sinks.

Introduction

African tropical moist forests (ATMF) play a vital role in global carbon cycling and climate regulation [1–6], covering large areas, and storing substantial amounts of carbon in soil and biomass [7–9]. These forests act as major biomass carbon sinks in structurally intact areas [1,10,11], making their conservation essential for mitigating climate change and preserving biodiversity [12–15]. However, growing food and energy demands [2,16–18] have accelerated biomass extraction and land conversion to agriculture, releasing carbon from vegetation and soil [18,19]. Additionally, the ability of structurally intact African forests to sequester carbon may be reaching its saturation point [1,20,21]. Yet, despite the urgent need to understand the role of African moist forests in climate mitigation, this region remains notoriously understudied [3].

Effectively tackling climate change necessitates integrating tropical moist forests into Nationally Determined Contributions (NDCs) of African countries [22,23]. Previous studies have primarily focused on continental [5,24–27], regional [28–30], and to a lesser degree national carbon flux estimates [10,31,32]. However, in ATMF-rich countries, accurate national-scale reporting remains challenging due to data gaps [3] and discrepancies between ground observations [1], satellite data [10,30,31,33,34], and models [35–38], spanning various spatial and temporal scales. The most recent endeavor to quantify African continental-scale carbon fluxes used vegetation models (TRENDY v9 and aDGVM), five atmospheric inversions, and five data-driven remotely sensed products, as part of the RECCAP2 project [28]. However, TRENDY v9 lacks the latest calibrations and process representations, while the relatively small number of atmospheric inversions likely makes uncertainty assessment incomplete. Furthermore, field data in primary forests used to calibrate and validate satellite biomass maps is relatively limited, as well as repeated measurements to explicitly inform temporal biomass changes [39–43]. Yet, this limited use of field data stands in contrast to the growing availability of repeated tree measurements from permanent inventory plots, which enable constraining important fluxes such as intact forest carbon uptake through tree growth and carbon loss through tree mortality over time [1,21,44–49].

The absence of accurate national carbon flux data is problematic because it hampers the assessment of ATMF countries' past and present contributions to climate change through incomplete NDCs [50,51], making regional and global carbon balances uncertain [4,5,25,28,36,50,52,53]. It also impairs designing and implementing effective climate and biodiversity policies, including forest monitoring and conservation initiatives [54]. Addressing this gap requires a rigorous, comprehensive analysis of national carbon fluxes in ATMF countries to improve scientific understanding of their role in global climate dynamics and inform policy frameworks.

Here, we present a rigorous national-scale assessment of individual carbon fluxes and the net ecosystem exchange (NEE or summed non-fossil fuel land carbon fluxes [55]), as well as their associated uncertainties for 18 West and Central African ATMF countries (**Figure 1**; **Supplementary Figure 1**; **Supplementary Table 1**), encompassing ~99% of Africa's tropical moist forests [56]. We focused on the period 2015-2019 which offers the greatest concentration of observational constraints. We combined a diverse range of state-of-the-art, model-based, and data-informed approaches. Our bottom-up approaches separately estimate national net carbon removals of intact forests and emissions from land-use change. Carbon removals by structurally intact woody ecosystems (ΔC_{intact}) are estimated using several independent approaches including: above- and belowground biomass carbon stock data upscaled from a large database of forest plot measurements not previously used in national-, regional- or continental-scale budgets [1]; a Bayesian CARbon DAta–MOdel fraMework (CARDAMOM) [57], that is uniquely able to propagate pixel level observations and their uncertainties into a systemic carbon cycle analysis; and a large ensemble of 17 Dynamic Global Vegetation Models (DGVMs) from TRENDY v11, the first TRENDY iteration where the multi-model ensemble provided the land sink for the main global carbon budget [57–59]. Following IPCC Tier 1 guidelines [60] and due to high uncertainty in tropical regions [55], soil, deadwood, and litter pools were assumed unchanged for ΔC_{intact}. Land-use change emissions were estimated using an ensemble of 18 DGVMs [57–59], CARDAMOM [57], three bookkeeping models [61–63], and satellite data [32,60,64,65], capturing removals from forest regrowth and emissions from deforestation, degradation, and fire. We completed national carbon balances by accounting for lateral river [36,66] and trade [67] fluxes, carbon storage in inland water sediments [68,69], and coastal vegetation removals [70–73].

We derived our top-down NEE estimates from an ensemble of 14 atmospheric CO_2 inversions [36,66], nearly three times as many used in the recent RECCAP2 analysis of Africa [28] offering a more complete quantification of NEE uncertainty. These top-down estimates of net land carbon fluxes implicitly include all carbon fluxes across space and time. These models, primarily Bayesian, reduce discrepancies between observed (from satellites or ground-based) and modeled atmospheric CO_2 from atmospheric transport models which incorporate prior land flux information [27].

Ultimately, to assess the role of African ecosystems in the carbon balance, we compared bottom-up and top-down national-scale NEE estimates with fossil fuel emissions [26]. The rigor of our analysis comes by utilizing a more diverse and greater number of independent estimates (than either RECCAP2 [28] or the Global Carbon Budget (GCB) [36]), but also by using a Monte Carlo approach to propagating their collective uncertainty providing a probabilistic estimate of whether a given nation represents a net carbon source or sink.

Results

Bottom-up estimates of carbon removals by structurally intact terrestrial ecosystems

To quantify carbon removals by structurally intact (primarily woody) terrestrial ecosystems (ΔC_{intact}, i.e., forests and woodlands without recent events of deforestation, degradation, or regrowth [56,74,75]) across 18 ATMF countries, we estimated annual changes in live biomass carbon stocks using upscaled forest plot measurements [1], CARDAMOM [57], and 17 DGVMs [58,59]. Together, these three approaches estimated total carbon removals of -203 ± 68.1 TgC yr^{-1} (median ± interquartile range) across all ATMF countries during 2015-2019 (**Figure 2A**; **Supplementary Figure 2**).

The Congo Basin accounted for the largest share of removals (-112.9 ± 64.9 TgC yr^{-1}) (**Figure 2A**), driven by extensive and productive, structurally intact forests and woodlands in the Democratic Republic of the Congo (COD) (-81.7 ± 64.2 TgC yr^{-1}) and Central African Republic (CAF) (-24.4 ± 9.6 TgC yr^{-1}) (**Supplementary Figure 3**). Atlantic Central Africa and West-Africa contributed less to removals at -52.5 ± 18.3 TgC yr^{-1} and -37.5 ± 9.5 TgC yr^{-1}, respectively, with maximum removals in Cameroon (-27.1 ± 7.8 TgC yr^{-1}) and Ivory Coast (-8.5 ± 5.8 TgC yr^{-1}), reflecting smaller forested areas relative to the Congo Basin.

Per-hectare, structurally intact woody ecosystems sequestered a similar amount of atmospheric CO_2 in countries in the Congo Basin (e.g., COD: -0.6 ± 0.2 MgC ha^{-1} yr^{1}) and Atlantic Central Africa (e.g., Gabon: -0.4 ± 0.4 MgC ha^{-1} yr^{-1}) (**Figure 2B**). We observed lower carbon removals per hectare in smaller Central African (e.g., Burundi and Rwanda) and West-African countries (e.g., Guinea-Bissau, Togo, and Sierra Leone), where less productive ecosystems such as shrublands and open woodlands were more common than highly productive forests (**Supplementary Table 1**).

Upscaled forest plot measurements and DGVMs showed consistent carbon uptake in intact woody ecosystems across all countries (**Figure 2; Supplementary Figure 4**). In contrast, CARDAMOM indicated localized decreases in biomass carbon stocks, particularly in central Congo Basin (e.g., COD), parts of Atlantic Central Africa (e.g., Gabon, Republic of the Congo, and

Equatorial-Guinea), and West-Africa (e.g., Ivory Coast) due to climate-driven variability (**Supplementary Figure 5**).

Bottom-up estimates of other components of net ecosystem exchange

Apart from ΔC_{intact}, we quantified other non-fossil fuel carbon fluxes as part of our bottom-up approach. These are land-use change fluxes (F_{LUC}) [32,60,64,65], aquatic ecosystem fluxes ($F_{aquatic}$), and fluxes from trade in wood and crops ($F_{crop+wood}$) [67] (**Figure 3**). $F_{aquatic}$ encompassed organic carbon export from rivers to oceans [66,76–79], burial in inland sediments [68,69], and sequestration by coastal vegetation [70–73]. Together with carbon removals by structurally intact ecosystems (ΔC_{intact}), these fluxes comprise the net ecosystem exchange: $NEE = \Delta C_{intact} + F_{aquatic} + F_{LUC} + F_{crop+wood}$ [55]. We found that aquatic ecosystems were a net carbon sink across all ATMF countries together, at -83.1 ± 6.2 TgC yr^{-1} (**Figure 3**). This was primarily due to sediment burial and coastal vegetation uptake, with the largest contributions in Nigeria and the Democratic Republic of the Congo, reflecting the influence of the Niger and Congo river systems (**Supplementary Figure 6**).

Land-use change emissions were highest in the Congo Basin (235.5 ± 94.5 TgC yr^{-1}) (**Figure 3A**), mainly driven by substantial forest loss and degradation in the Democratic Republic of the Congo (166.5 ± 64.8 TgC yr^{-1}) and Central African Republic (65 ± 68.5 TgC yr^{-1}) (**Supplementary Figure 7**). Both countries were the largest national gross emitters and among the highest emitters per hectare (**Supplementary Table 2**). West-Africa followed with 77.8 ± 29.8 TgC yr^{-1}, with a maximum in Ivory Coast (17.6 ± 10.3 TgC yr^{-1}) (**Figure 3A**). In West-African countries such as Sierra Leone and Liberia, per-hectare land-use change emissions were the highest of all 18 countries, indicating a high degree of forest disturbance (**Supplementary Table 2**; **Supplementary Figure 7**). In contrast, Atlantic Central Africa had the lowest absolute (22.9 ± 15.1 TgC yr^{-1}) and per-hectare land-use change emissions (0.1 ± 0.3 MgC ha^{-1} yr^{-1}) (**Figure 3A**), with particularly low values in Gabon (2.6 ± 7.1 TgC yr^{-1} and 0.2 ± 0.1MgC ha^{-1} yr^{-1}) (**Figure 3B**; **Supplementary Table 2**).

Trade-related carbon fluxes were generally negligible relative to other carbon fluxes, but mostly contributed net emissions in countries with high imports such as Nigeria (**Figure 3A; Supplementary Table 2**).

Comparing bottom-up and top-down net ecosystem exchange estimates

We compared our bottom-up NEE estimates (**Figure 3**) with top-down NEE derived from 14 atmospheric inversions [36,66] corrected for lateral fluxes (**Supplementary Figure 8**). We found that, between 2015 and 2019, both approaches suggested that all 18 ATMF countries together were a small carbon source or near-neutral given substantial uncertainty, with the bottom-up estimate at 57.4 ± 121.4 TgC yr^{-1} (median ± interquartile range; 60% certainty of being a net source) and the top-down estimate at 99.4 ± 164.5 TgC yr^{-1} (66% certainty of being a net source) (**Figure 4A; Supplementary Table 2**). The difference between the two approaches was 41.7 ± 204.4 TgC yr^{-1}, with the highest imbalance observed in West-Africa (**Supplementary Table 2**). However, this difference was not statistically significant in any country or region due to high uncertainty (P-value>0.05).

Both methods indicated that Atlantic Central Africa was likely a net carbon sink, with 58% and 74% certainty for the bottom-up and top-down approach, respectively (**Supplementary Table 2**). By contrast, the Congo Basin appeared near-neutral or a net source (52% certainty for ensemble) (**Figure 4A**) due to substantial land-use change emissions (**Figure 3**). There was no consensus between the bottom-up and top-down estimates for West-Africa, where the bottom-up approach suggested carbon neutrality due to high past deforestation (**Supplementary Figure 3B**), while top-down inversions indicated a net source with 84% certainty (**Supplementary Table 2**). At the national level, both approaches suggested that Gabon was a net sink (at -14.2 ± 12.9 TgC yr^{-1} with 70% certainty for bottom-up approach and -12.3 ± 14.1 TgC yr^{-1} with 63% certainty for top-down approach), while most ATMF countries were near-neutral (**Supplementary Table 2**). In contrast, the Democratic Republic of the Congo and Central African Republic were potentially net sources with 37% and 61% certainty for the ensemble NEE (**Supplementary Table 2**), but uncertainty intervals overlapped the carbon source/sink boundary (**Figure 4A**). No country

or region showed a statistically significant difference from zero due to high uncertainty (P-value>0.05).

Contrasting the net ecosystem exchange with fossil fuel emissions

Fossil fuel emissions were minor relative to other carbon fluxes, with only Nigeria, Ivory Coast, Ghana, and Cameroon exceeding 2 TgC yr^{-1} (**Table 1**). West-Africa had the highest fossil fuel emissions (41.9 ± 1.6 TgC yr^{-1}), dominated by Nigeria which was the highest national emitter at 31.2 ± 1.6 TgC yr^{-1}. In contrast, fossil fuel emissions were lower in Atlantic Central Africa (7.8 ± 0.2 TgC yr^{-1}) and the Congo Basin (2.8 ± 0.1 TgC yr^{-1}), led by Cameroon and the Republic of the Congo, respectively. The lowest fossil fuel emitters were Central African Republic, Guinea-Bissau, and Burundi (each at 0.1 TgC yr^{-1}).

In the Congo Basin and Atlantic Central Africa, non-fossil fuel carbon fluxes surpassed fossil fuel emissions, particularly in the Democratic Republic of the Congo and Central African Republic, where energy is predominantly derived from fuelwood and charcoal instead of fossil fuels. West-Africa exhibited comparable fossil and non-fossil fuel carbon fluxes, as observed in Nigeria (**Table 1**). Overall, from 2015 to 2019, non-fossil fuel land carbon fluxes dominated the ATMF countries' carbon balances, characterized by substantial removals from intact woody ecosystems and high emissions from land-use change.

Discussion

Substantial carbon removals nearly offset land-use change emissions in African tropical moist forests

Our results suggested that, for 2015-2019, the 18 ATMF countries were collectively likely a small net carbon source or near-neutral given the high uncertainty. While land-use change emissions were substantial, particularly in the Democratic Republic of the Congo and Central African Republic, they were largely offset by carbon removals in intact woody ecosystems, especially within Atlantic Central Africa's countries. Lateral carbon fluxes via riverine export and trade were minimal compared to other land-atmosphere exchanges.

Intact woody ecosystems in tropical Africa sequestered an estimated -203 ± 68.1 TgC yr^{-1} from the atmosphere during 2015-2019, with most removals occurring in the Congo Basin hosting the second-largest tropical rainforest globally [1,48]. Our estimate was slightly lower than previous average carbon removal estimates for tropical Africa (-258 ± 128 TgC yr^{-1}) [1,5,10,24,28,30,31,80] and much lower than estimates for continental Africa (-516 ± 245 TgC yr^{-1}) [4,21,25,28,48,53,63] (**Supplementary Figure 9**) due to three potential reasons. First, we focused on ATMF countries, excluding woodlands in Eastern and Southern Africa [28,81]. Second, CARDAMOM yielded lower biomass carbon removals in intact woody ecosystems than other approaches (**Supplementary Figure 4**), including biomass declines in the central Congo Basin, contrasting with increases shown by upscaled plot measurements and DGVM [82]. This could reflect CARDAMOM's sensitivity to moisture stress and reliance on remote sensing data [30,83], which may enable detection of biomass losses from climatic extremes such as the 2015-2016 El Niño [33], likely not captured by other models [40] or forest plot datasets limited to the period 1990-2015 [1]. Third, our bottom-up approach excluded litter, deadwood, and soil carbon fluxes in intact ecosystems (see below).

Carbon emissions from land-use change were substantial, nearly offsetting carbon removals by forest productivity in ATMF countries. Land-use change was the primary source of emissions in these countries [10,31,84], with the majority occurring in the Democratic Republic of the Congo resulting from forest loss and degradation due to smallholder clearing, mining, road construction, and logging [16,18,30,85,86]. We estimate total land-use change emissions in ATMF

countries at 336.2 ± 100.2 TgC yr^{-1}, which is slightly higher than previous studies in tropical Africa [5,8,10,18,28,30,31,80,84,87–91] (mean ± standard deviation: 220 ± 113 TgC yr^{-1}) and similar to estimates for continental Africa [4,18,24,25,28,53,55,63,92,93] (341 ± 110 TgC yr^{-1}) (**Supplementary Figure 9**). This discrepancy likely stems from methodological differences for handling selective logging, forest recovery, and fire across methods, which have been underrepresented in previous assessments [94,95].

Uncertainties conceal net carbon sink or source

Methodological limitations contributed to large uncertainties and inconsistencies between approaches, preventing a clear determination of whether ATMF countries were statistically significant net carbon sources, sinks, or neutral (**Figure 4**). Due to high uncertainty [96], our bottom-up approach assumed soil, deadwood, and litter carbon stocks constant in intact terrestrial ecosystems, aligning with IPCC Tier 1 guidelines [22], but unlike other studies [4,5,24,25,28,53,63]. Incorporating soil, deadwood, and litter in our bottom-up analysis increased estimated removals by 40% for the whole region (from -203 ± 68.1 TgC yr^{-1} to -284.7 ± 73.2 TgC yr^{-1}), potentially shifting the region from near-neutral to a modest net sink (**Supplementary Figure 10**). However, despite similar total removals across methods [28], soil, deadwood, and litter contributed little to total carbon changes in forest plot data (from limited FAO data [97]) compared to DGVMs and CARDAMOM (**Supplementary Figure 10**). Field experiments assessing the change in soil, deadwood, and litter carbon stocks in response to warming in tropical forests are limited to Central America, suggesting that these pools are closely interlinked [98–101] (however, Sayer et al. [102] showed no increases in soil carbon stocks after 15 years of doubled litter inputs) and highly sensitive to environmental changes with limited short-term acclimation, potentially triggering positive earth-atmosphere feedbacks [103,104]. However, a recent study combining atmospheric inversions and satellite-based biomass maps identified Africa as a large net soil and litter carbon sink at -0.34 ± 0.14 Pg C yr^{-1} and a deadwood sink at -0.01 ± 0.01 Pg C yr^{-1} due to carbon uptake in old-growth forests and croplands [105], yet experiments on soil, deadwood, and litter carbon responses to environmental change in undisturbed forests and woodlands remain scarce in tropical Africa.

In Africa, smallholder-driven land-use change causes subtle forest disturbances often undetectable by satellite images [74] due to coarse resolution and optical limitations [106], leading to underestimated emissions from degradation [107], deforestation [74], and fires [95]. Process-based and bookkeeping models [108,109] also face constraints, including inadequate carbon density maps [109] which are often biased [110] due to limitations in satellite data (e.g., cloudiness for optical data [111,112]), allometric relations (particularly with LiDAR) [113], topographic complexity, and sparse field data in regrowing [114,115] and old-growth moist forests [46], dry forests [4,21,81,116], non-forest ecosystems [4], and managed forests [117] (especially in the Congo Basin [41]). Additionally, bookkeeping models tend to underrepresent land-use dynamics such as shifting cultivation and even deforestation, as they rely on inadequate land-use change datasets [118,119] like LUH2 (BLUE), FAO statistics (H&C2023), or combinations thereof (OSCAR) [120].

Carbon flux estimates from DGVMs, such as those in TRENDY, are highly uncertain in tropical ecosystems [109,121]. DGVMs use a limited set of plant function types (PFT), such as tropical moist forests [122], often calibrated at few sites, with the assumption that PFT parameters remain spatially and temporally invariant, despite evidence to the contrary [123]. Additionally, key land-use processes, including (peat) fires, irrigation, tillage, erosion, nitrogen fertilization, natural disturbances, and grazing, are inconsistently represented across DGVMs [26,119], and integrating these likely increases rather than reduces uncertainty in DGVMs. The absence of eddy covariance flux measurements in Equatorial Africa [124] further limits the ability to constrain these models [5]. Despite limitations regarding bottom-up fluxes, our estimates broadly aligned with National Greenhouse Gas Inventories (NGHGIs) [125] (**Supplementary Figure 11**). However, alternative bottom-up approaches, such as X-BASE flux tower data (corrected for emission components) [126] and SMOS-LVOD aboveground biomass carbon flux data [30,34], indicated larger net carbon sinks in the Congo Basin and divergent regional NEE for West-Africa classified as near-neutral by SMOS-LVOD but a substantial source by X-BASE (**Supplementary Figure 11**), highlighting the discrepancies between various bottom-up approaches.

Top-down atmospheric CO_2 inversions implicitly capture all total net surface-atmosphere carbon fluxes, whereas bottom-up approaches exclude several components. Most notably, we decided to exclude soil, deadwood, and litter carbon fluxes in structurally intact ecosystems due

to the high uncertainty regarding the dynamics of these carbon pools in tropical forests due to sparse data. Emissions from fine-scale land-use change, such as small fires, forest edge effects, and selective logging are also likely underestimated in bottom-up approaches [95,110]. These processes are widespread in smallholder agricultural landscapes and forest-savanna transition zones across tropical Africa, yet are poorly represented in current land-use and fire datasets. In contrast, such fluxes are likely to be implicitly incorporated into inversion-based NEE estimates [27,127], which contributes to the divergence between top-down and bottom-up approaches [128]. However, atmospheric inversions cannot explicitly partition net fluxes into their gross underlying sources and sinks, such as fossil fuel emissions versus biogenic land carbon fluxes [27,82,129]. Additional uncertainties arise from multiple methodological factors, including the type and quality of assimilated observations (satellites versus ground-based), the sparsity of high-quality *in situ* atmospheric CO_2 measurements across most of Africa, limitations in atmospheric transport models, and uncertainties in the magnitude and spatial-temporal structure of prior land carbon fluxes (**Supplementary Table 3**) [27,130]. Consequently, while inversion approaches provide more stable estimates at continental or large regional scales, the magnitude and spatial distribution of NEE remains highly uncertain at national and subregional scales in these regions with limited observational coverage [131].

These limitations are particularly evident in West-Africa, where bottom-up estimates suggest near carbon neutrality, whereas inversion-based approaches indicate a net carbon source. Beyond sparse surface (but not satellite) CO_2 observations and uncertainties in prior fluxes [27,130], atmospheric transport modeling is especially challenging in this region. Circulation is strongly governed by the West-African monsoon, which organizes air flow across steep climatic gradients from the humid Upper Guinean forests along the Atlantic coast to the semi-arid Sahel interior [132,133]. Transport simulations and satellite retrievals used in inversions are further complicated by pronounced land-cover heterogeneity and dynamics (e.g., croplands, grasslands, savannas, and forest mosaics), sea surface temperature variability linked to Guinea Coast upwelling, Saharan dust and biomass burning aerosols, cloud formation, and deep convection [134–136].

Persistent uncertainties in regional net carbon fluxes highlight the need for enhanced carbon monitoring in humid African tropics. Constraining net carbon fluxes requires regular atmospheric CO_2 sampling through aircraft campaigns [137]. To decompose net carbon fluxes into individual sources and sinks, an integrated monitoring network should be established, including (1) distributed forest inventory plots tracking live biomass, soil, deadwood, and litter carbon stocks to quantify regrowing and old-growth forest carbon sinks [1,46,138], (2) eddy covariance flux towers to measure net ecosystem fluxes [124] including in understudied ecosystems such as carbon-rich peatlands (e.g., Cuvette Central) [139], and (3) 'supersites' combining field and airborne biomass data for high-resolution land-use and carbon density maps [140]. These *in situ* data can improve bookkeeping, dynamic vegetation, and inversion models. By ranking regions according to the uncertainty in NEE and bottom-up carbon flux components, we identified the Congo Basin, particularly the Democratic Republic of the Congo and Central African Republic due to their vast forest extents and ongoing land-use changes, as priority regions for future sampling campaigns to better constraints on land-use change fluxes and net carbon removals in intact tropical forests and woodlands (**Supplementary Figure 12**). Lastly, expanding monitoring to other greenhouse gases, such as CH_4 and N_2O, is essential for a comprehensive regional greenhouse gas budget [139,141].

Environmental policies matter

We revealed that ATMF countries exhibited high land-use carbon emissions and ecosystem carbon removals, while fossil fuel emissions remained relatively low [26] (**Supplementary Figure 13**), especially in the Congo Basin [17]. Differences in carbon balances across ATMF countries were at least partly reflecting national environmental policies. For example, Gabon, known for strong forest conservation policies as a High-Forest, Low-Deforestation country [3,54], had low land-use emissions and high removals per hectare, likely resulting in a net sink for the bottom-up (at -14.2 ± 12.9 TgC yr^{-1}) and top-down approach (at -12.3 ± 14.1 TgC yr^{-1}) with a certainty of 70% and 63%, respectively. In contrast, countries such as CAF and COD, with less stringent policies, showed high per-hectare emissions and removals, potentially making them net carbon sources or near-neutral [54,142]. This underscores the potential of forest conservation policies in ATMF countries such as the Democratic Republic of the Congo

and Central African Republic to conserve structurally intact ecosystems and reduce land-use change emissions. Future research could examine the causal relationships between national environmental policies and carbon balances across African tropical moist countries, accounting for socio-economic differences, to improve the identification of the drivers of variation in national-scale carbon emissions and sources, for example, by drawing on approaches used in national-scale assessments of REDD+ program impacts on forest carbon stocks [143,144].

Moreover, intact forest ecosystems tend to be spatially clustered (**Supplementary Figure 3**), highlighting that regional-scale carbon flux estimates can mask heterogeneity in land-use cover and ecosystem intactness. Small countries with heavily disturbed forests, such as Sierra Leone and Guinea, exhibit high per-hectare net carbon emissions but contribute relatively little to regional carbon emissions because of their limited spatial extent and low, yet highly heterogenous, ecosystem intactness (**Supplementary Figure 14**). In contrast, large countries such as the Democratic Republic of the Congo contribute substantially to regional net carbon emissions, while having low per-hectare emission rates due to extensive areas of relatively intact forests with limited spatial heterogeneity (**Supplementary Figure 14**). These contrasting patterns demonstrate that conservation policies should jointly consider absolute carbon fluxes, per-area emission or removal intensity, and the spatial extent and clustering of ecosystem intactness. Integrating these dimensions, for example within baseline frameworks such as those applied in the Tropical Forest Forever Facility (TFFF) Initiative [145], can help balance policy considerations between countries with high per-area impacts but small absolute contributions and those with large absolute emissions because of extensive forest area.

Our findings highlight the urgency to conserve structurally intact ecosystems such as forests and woodlands to mitigate global warming (distinguishing between passive and active carbon sinks) [13], support biodiversity [146], and maintain ecosystem services, including local climatic buffering [147] and water provisioning [148]. Given large projected population growth in Central Africa over the next decades [149], a major challenge will be to reconcile forest conservation with regional food security [150]. This underpins the paramount importance of implementing policies that promote sustainable, low carbon economic development. ATMF, whose emissions are dominated by land-use change, contrast sharply with current and historically high fossil-fuel-

emitters in the Global North (**Supplementary Figure 13**). Protecting intact forests while supporting local livelihoods will require international support that empowers African tropical countries to strengthen their local research, monitoring, and forest management, with active participation of indigenous communities (e.g., through financial initiatives such as TFFF [145]). Support reflecting current and historical global emission asymmetries can help reconciling forest conservation objectives with development priorities, ensuring that forest stewardship is guided by local knowledge and needs. At the same time, it is critically urgent to reduce global anthropogenic greenhouse gas emissions to mitigate climate-driven carbon losses [151]. Despite remaining uncertainties, our national carbon flux estimates provide a foundation for sustainable policies fostering both local livelihoods and effective climate and conservation strategies in tropical Africa's carbon-rich, biodiverse countries.

Methods

Temporal and geographic coverage

We limited our study period to the ten years between 2015 and 2019, covering the temporal availability of all observation and model data products (**Supplementary Table 4**). We quantified carbon fluxes within three different types of terrestrial ecosystems: 'forests' (tree cover greater than 30%, canopy >5m), 'woodlands' (also referred to as 'woody non-forests'; tree cover 5-30%), and 'other ecosystems' (grasslands, wetlands, settlements, croplands/natural vegetation mosaics, and barren areas). The extent of each of these ecosystems was based on the land use cover map from the Moderate Resolution Imaging Spectroradiometer (MODIS) MCD12Q1.061 [152] for the year 2015 (**Supplementary Figure 3; Supplementary Table 1; Supplementary Table 4**).

We calculated national fluxes for 18 countries (**Supplementary Table 4**). Country boundaries were extracted from the Global Administrative Unit Layers (GAUL) [153]. Analysis of remote sensing products was performed in Google Earth Engine [154]. Further quantification of carbon fluxes (e.g., Dynamic Global Vegetation Models, CARDAMOM, inversion models, and Monte Carlo methods) and plotting was done in R v4.4.0 [155].

Bottom-up national net ecosystem exchange

Using a bottom-up framework, national-level net ecosystem exchange (NEE) was calculated by summing non-fossil fuel land carbon fluxes (F) (**Equation 1**; **Supplementary Figure 1**) (in TgC yr^{-1}) related to structurally intact terrestrial ecosystems (ΔC_{intact}), land-use change (F_{LUC}), aquatic ecosystems ($F_{aquatic}$), and lateral import and export through trade in crops and wood ($F_{crop+wood}$). $F_{aquatic}$ was the net aquatic flux calculated by summing organic carbon export by rivers to oceans (F_{river}), carbon burial in sediment in inland waters (F_{burial}), and carbon assimilated by coastal vegetation ($F_{coastal\ vegetationl}$). As our fluxes are to be interpreted from an atmospheric perspective, the sign convention is that carbon removals are negative values (ecosystem acts as a carbon sink) and carbon emissions are positive values (ecosystem acts as a carbon source). To convert carbon fluxes per area into absolute fluxes, we multiplied the carbon

flux per area by the pixel surface area. We then calculated national-scale carbon fluxes by summing the pixels with absolute fluxes per country.

$$\mathrm{NEE} = \Delta \mathrm{C}_{\mathrm{intact}} + \mathrm{F}_{\mathrm{LUC}} + \mathrm{F}_{\mathrm{aquatic}} + \mathrm{F}_{\mathrm{crop+wood}} \text{ (**Equation 1**)}$$

We quantified each carbon flux component and its uncertainty using a Monte Carlo approach [156]. For each carbon flux assessed with two or more estimates, we calculated the flux by taking the median of the medians from 10,000 randomly generated Gaussian distributions (each distribution with n = 1,000) based on the mean and standard deviation of each individual estimate per flux. Similarly, the uncertainty was estimated by taking the median of the inter-quartile ranges of all generated distributions. We used the internal error for carbon fluxes with only one estimate (e.g., $\mathrm{F}_{\mathrm{crop+wood}}$). The uncertainty of NEE was calculated using error propagation.

After calculating national net carbon fluxes and components, we also quantified carbon fluxes at the regional level (**Supplementary Table 1**) by summing national carbon fluxes (**Figure 3**) for countries in West-Africa, Atlantic Central Africa, Congo Basin, and the whole region (all 18 African countries together). The uncertainty was quantified based on propagating national-level uncertainties. Carbon flux components and their uncertainties are described separately in the following sections.

Carbon removal by structurally intact and other terrestrial ecosystems ($\Delta \mathrm{C}_{\mathrm{intact}}$)

To quantify the carbon flux in tropical terrestrial ecosystems at a national level ($\Delta \mathrm{C}_{\mathrm{intact}}$) as a response to a changing atmospheric CO_2 and climate, we estimated net carbon fluxes due to changes in above- and belowground (coarse roots) biomass carbon stocks in structurally intact woody (i.e., forests and woodlands) ($\Delta \mathrm{C}_{\mathrm{intact\ FW}}$) and other terrestrial ecosystems ($\Delta \mathrm{C}_{\mathrm{intact\ other}}$). Throughout the process, we assumed that soil, deadwood, and litter pools did not change because of their high uncertainty in tropical regions [55] and in line with the IPCC Tier 1 assumption of no net changes to non-biomass pools in 'undisturbed' ecosystems [60]. We reported carbon fluxes in tropical terrestrial ecosystems as one component $\Delta \mathrm{C}_{\mathrm{intact}}$, but carbon removals were

also quantified per biome (**Supplementary Figure 2**). The uncertainty was calculated using error propagation based on the Monte Carlo interquartile ranges.

$$\Delta C_{intact} = \Delta C_{intact\ FW} + \Delta C_{intact\ other}$$ (**Equation 2**)

Carbon removal by structurally intact forests and woodlands ($\Delta C_{intact\ FW}$)

Mapping structurally intact forests and woodlands

To calculate carbon removals by structurally intact forests and woodlands (i.e. with no recent event of land-use change), we generated a map with ecosystem intactness following Rosan et al. [157] by calculating the fraction of each pixel that did not undergo any recent forest degradation, deforestation, or forest regrowth during the period with available land-use change data (i.e., 1990-2019) using two forest conversion maps: Global Forest Watch (GFW) (version 1.9) [74] and Tropical Moist Forest (TMF) (version 1 2021) [56] (**Supplementary Figure 3**). An ecosystem intactness of '0' indicates the absence of structurally intact forests and woodlands within a pixel, while '1' implies that the whole pixel is covered by structurally intact forests and woodlands.

Upscaled forest plot measurements (AfriTRON)

We generated a field data-driven map of the carbon removal by structurally intact woody ecosystems [152] (**Supplementary Figure 5**). We adopted methods from Hubau et al. [1], who used linear mixed modeling to link environmental variables and the net biomass carbon removal by African tropical moist rainforests based on a permanent inventory plot data from the African Tropical Rainforest Observation Network (AfriTRON) [1], containing 244 repeatedly censused plots in humid tropical rainforest with a total plot area of 277.9 hectares. Since this data only covers changes in stem, branch, and leaf biomass carbon stocks, we assumed that carbon removal and emission from other carbon components such as fine roots, fruits, and seeds was in steady state. We included belowground carbon (i.e., coarse roots) by adding 25% and 49% of aboveground biomass carbon in African forests [48] and woodlands [32], respectively.

By combining spatial maps of the environmental variables with the coefficients of the linear mixed models from Hubau et al. [1], we produced annual maps of $\Delta C_{intact\ FW}$ per area (in MgC ha^{-1} yr^{-1}) in structurally intact forests at 0.01° for 2015-2019. The environmental variables

consisted of atmospheric CO_2 concentrations (from the Mauna Loa record: Global Monitoring Laboratory - Carbon Cycle Greenhouse Gases (noaa.gov)), mean annual temperatures (from the Climate Research Unit CRU TS v4.07 [158] combined with WorldClim v2 [159] to downscale CRU to resolution 1 km), mean climatic water deficit (calculated using data on evapotranspiration [1] and monthly precipitation from the Tropical Rainfall Measurement Mission (TRMM) data v7 [160], and WorldClim v2 [159] to downscale TRMM to resolution 1 km), wood density (kriging of plot-level mean wood densities from Hubau et al. [1]), and the carbon residence time (estimated based on dividing the mean aboveground carbon density from five maps [7–9,161,162] by the spatially predicted carbon removals from Hubau et al. [1]).

In structurally intact woodlands, we calculated carbon removals per area by applying a mean annual percentage change to the carbon density (in MgC ha^{-1}). The annual percentage change was calculated by averaging the net aboveground carbon removal divided by the initial annual aboveground carbon stocks in forests across the whole studied for every year between 2015 and 2019. To calculate $\Delta C_{\text{intact FW}}$ we multiplied the map of the $\Delta C_{\text{intact FW}}$ per area by the fraction with structurally intact ecosystems at resolution 0.01° (**Supplementary Figure 3**). Since the AfriTRON plot network only covered old-growth tropical moist forests, we excluded forest plantations [163].

We produced uncertainty maps of carbon removals by combining the variance-covariance matrix of the model coefficients with the maps of the environmental variables using the standard formula for propagated prediction variance ($x^T V x$ where x is the vector of predicted values and V is the variance-covariance matrix of the fitted linear mixed models) (**Supplementary Figure 5**). We derived the uncertainty bounds on $\Delta C_{\text{intact FW}}$ by propagating upper and lower bounds of carbon gains and losses, that is, the upper net flux bound was computed as upper gains minus upper losses, and the lower net flux bound as lower gains minus lower losses [1]. Since the linear mixed models from Hubau et al. [1] only included plot data in humid tropical rainforests, we assumed that the uncertainty in woodlands equaled the mean relative standard deviation in forests over the whole studied region (rel. sd. ≈ 71%). To calculate the uncertainty of the national-level $\Delta C_{\text{intact FW}}$, we computed the standard error as half the difference between the spatially integrated upper and lower $\Delta C_{\text{intact FW}}$, bounds across all pixels per country.

Dynamic Global Vegetation Models (TRENDY v11)

$\Delta C_{\text{intact FW}}$ was also quantified using the Dynamic Global Vegetation Models (DGVMs) from TRENDY v11 [58,59] (ensemble of 17 models). We calculated the Monte Carlo average of the annual change in above- and belowground vegetation carbon stocks between the consecutive years 2015 and 2019 of the 17 models (**Supplementary Figure 4**). To extract forests and woodlands, we rescaled all models to resolution 0.5° (highest model resolution) and used a forest and woodland mask [152] (**Supplementary Figure 3**). We used scenario S2, in which changes in the vegetation carbon density due to climate change and increased atmospheric carbon dioxide concentrations were accounted for, but changes in the land-use cover were not considered. To prevent overestimating carbon removals [164], we multiplied $\Delta C_{\text{intact FW}}$ by the degree of intactness in forests and woodlands at resolution 0.5° (**Supplementary Figure 3**). The uncertainty was quantified by calculating the Monte Carlo standard deviation based on the 17 model estimates. Since including ecosystems such as agricultural land which potentially act as net carbon sources or neutral, it is likely that $\Delta C_{\text{intact FW}}$ is underestimated using DGVMs.

CARbon DAta-MOdel fraMework (CARDAMOM)

We also used the CARbon DAta-MOdel fraMework (CARDAMOM) model-data fusion analysis (resolution 1°) [35] to estimate ΔC_{intact} (**Supplementary Figure 4**). CARDAMOM is a DGVM based on Bayesian calibration at pixel scale, using remote sensing information on woody biomass, canopy phenology and disturbance to generate a probabilistic analysis of terrestrial carbon fluxes [35]. In line with DGVMs (see above), we used the annual change in above- and belowground biomass carbon stocks of Scenario 2 for the consecutive year combinations between 2015 and 2019. After rescaling the resolution from 1° to 0.5°, we multiplied the net biomass carbon removal by the degree of intactness for each pixel. The uncertainty was based on the interquartile range.

Carbon removal by other terrestrial ecosystems ($\Delta C_{intact\ other}$)

We quantified carbon removals by other ecosystems ($\Delta C_{\text{intact other}}$) using the Monte Carlo average of CARDAMOM [35] and the TRENDY v11 model ensemble [58,59] from scenario S2 (see above). Since carbon removal estimates using upscaled forest plot measurements only accurately

represented carbon removals in forests and woodlands (see above), we also added $\Delta C_{\text{intact other}}$ to forest plot-based estimates of $\Delta C_{\text{intact FW}}$ by calculating the Monte Carlo mean and standard deviation of $\Delta C_{\text{intact other}}$ using CARDAMOM [35] and TRENDY v11 [58,59].

Sensitivity analysis regarding changes in litter, deadwood, and soil carbon pools

To quantify effects of excluding changes in litter, deadwood, and soil carbon pools on net carbon removals by structurally intact terrestrial ecosystems, we calculated total carbon stock changes for the three methods described above. For CARDAMOM [35] and TRENDY v11 [58,59], we used the Net Biome Productivity (representing total carbon stock changes) for Scenario 2, corrected for ecosystem intactness (see above). For the upscaled forest plot measurements, we included litter, deadwood, and soil carbon stock changes based on the latest available field data. We did not use model-based estimates for adding missing carbon pools to the estimate based on upscaled forest plot measurements to enable comparison between model predictions and field observations. We added litter and deadwood carbon stock changes by adding a fixed factor from the IPCC [165] to the biomass carbon changes considering elevational zones [166] and mean annual precipitation [159], assuming that litter carbon pools responded proportionally to biomass carbon stock changes [21]. Then, we accounted for soil carbon stock changes using area-based soil carbon stock change rates for African structurally intact forests [21] (-0.021 ± 0.021 MgC ha^{-1} yr^{-1}), assuming similar responses in structurally intact woodlands.

To estimate the relative importance of changes in each of the carbon pools (biomass, litter, deadwood, and soil), we quantified the median pixel-level percentage change in each carbon pool in relation to the total carbon stock changes for the three methods, as well as the median pixel-level percentage change of soil to biomass carbon pools (**Supplementary Figure 10A-C**). Additionally, we compared national- and regional-scale carbon removals considering changes in biomass versus total carbon stocks (**Supplementary Figure 10D**).

Carbon emission through land-use change (F_{LUC})

Carbon fluxes related to land-use change consisted of carbon emissions due to deforestation, forest degradation, and forest fires, as well as carbon removals due to forest

regrowth. To compute carbon fluxes due to land-use change (F_{LUC}), we used Dynamic Global Vegetation Models from TRENDY v11, CARDAMOM, bookkeeping models, and a remote sensing-based approach (**Supplementary Figure 15**). Carbon fluxes due to wood and crop harvesting were (implicitly) included in this flux component.

Dynamic Global Vegetation Models (TRENDY v11)

To quantify both direct and indirect land-use change emissions based on TRENDY v11 (ensemble of 18 models) [58,59], we calculated the difference in the Net Biome Production (overall land carbon flux) of scenarios S3 (accounting for changing atmospheric carbon dioxide concentrations, climate, and land-use) and S2 (accounting for changing atmospheric carbon dioxide concentrations and climate) for all 18 models at their original resolution (**Supplementary Figure 15C; Supplementary Figure 16**). Because carbon emissions due to fires are most likely underestimated by DGVMs, we removed fire emissions from each model. The national-scale F_{LUC} (excluding fire emissions) was computed by calculating the Monte Carlo mean of the 18 model estimates, and the standard deviation.

To quantify the observation-based fire emissions, we calculated the Monte Carlo mean and standard deviation of national-scale total CO_2 fire estimates from the Global Fire Assimilation System (GFAS) [167] and Global Fire Emissions Database v5 (GFEDv5) [168]. To avoid double-counting emissions due to deforestation and forest degradation, we subtracted forest fire emissions from GFEDv5 [168] from total mean fire emissions. The final national-scale F_{LUC} estimate was computed by correcting F_{LUC} by the fire emissions, with the uncertainty calculated based on error propagation.

CARbon DAta-MOdel fraMework (CARDAMOM)

Similar to DGVMs, we calculated F_{LUC} using CARDAMOM by subtracting the net biome production of Scenario 3 and 2 (**Supplementary Figure 15A**). To be consistent with DGVM approach, we used the observation-based fire emission estimates to complete the land-use change flux (see above). The uncertainty equaled the interquartile range.

Bookkeeping models

We used the Monte Carlo average and standard deviation of three bookkeeping models (BLUE [62], H&C2023 [63], and OSCAR [61]) from the Global Carbon Budget 2023 [26] to quantify land-use change fluxes for 2015-2019 for each nation (**Supplementary Figure 15B**).

Remote sensing

To estimate the land-use change fluxes based on remote sensing (**Supplementary Figure 7; Supplementary Figure 15A**), we considered carbon emissions from forest degradation (E_{FD}), deforestation (E_D), and fire (E_F), and carbon removal due to forest regrowth (R_R). We excluded changes in soil (except for deforestation), deadwood, and litter carbon pools due to the high uncertainty regarding these fluxes [55]. To quantify the land-use change fluxes and their uncertainty, we calculated the mean and standard deviation using a Monte Carlo approach. We compared our remote sensing-based carbon emission and removal estimates to other studies (**Supplementary Figure 9**).

$$F_{LUC} = R_R + E_{FD} + E_D + E_F \text{ (**Equation 3**)}$$

To calculate R_R, we combined biomass carbon recovery models with maps of forest regrowth from GFW [169] and TMF [56] (**Supplementary Figure 7**). TMF [56] contains annual regrowth data, while GFW [169] indicates cumulative forest regrowth for 2000-2020. We summed the carbon removal in forests and woodlands [152] with forest regrowth in each year for 1991-2019 from TMF [56] and for the whole period 2000-2020 from GFW [169] per country. We then calculated carbon removals due to forest regrowth by applying two methods. On the one hand, we applied the aboveground biomass carbon recovery models from Heinrich et al. [65] (uncertainty equaled the interquartile range) to forest gains. Belowground biomass carbon was added for forests and woodlands by adding of 25% and 49% of aboveground biomass carbon in forests [48] and woodlands [32], respectively. On the other hand, we used the map of above- and belowground biomass carbon recovery models of Cook-Patton et al. [64], which we rescaled to 0.00025° resolution to match the land-use-change maps. The uncertainty was estimated by applying error propagation to the uncertainty map [64]. Soil, deadwood, and litter carbon changes were excluded due to high uncertainty of recovery rates [170], Moreover, chronosequence studies in the central Congo Basin showed little variation in soil and litter carbon stocks across a successional gradient

[115,171,172]. Taken together, this resulted in four estimates of carbon removal by regrowing forests per country (two series of land-use-change maps and two methods of carbon recovery rates).

To calculate biomass carbon emissions from forest degradation (E_{FD}) and fire (E_F) due to land-use change, we used annual live above- and belowground biomass carbon maps from Xu et al. [32]. The uncertainty of the emission components equaled 10% of the emission estimates [32]. Carbon emissions due to deforestation (E_D) consisted of emissions in above-and belowground tree biomass carbon ($E_{D,\text{tree biomass}}$), in soil organic carbon in mineral soils ($E_{D,SOC}$), and in soil organic carbon in peatlands ($E_{D,peat}$).

$$E_D = E_{D,\text{tree biomass}} + E_{D,SOC} + E_{D,peat} \quad \textbf{(Equation 4)}$$

To compute $E_{D,\text{tree biomass}}$, we used the maps from Xu et al. [32] (uncertainty equaling 10% of the national estimate). $E_{D,SOC}$ was estimated by combining annual forest loss data from the Global Forest Watch (GFW) [74,75] and Tropical Moist Forest (TMF) [56] (resolution 0.00025°) with a map of soil organic carbon (SOC) stocks at depths 0-30 cm from SoilGrids version 2.0 [173]. To match the forest loss maps, we rescaled the SOC map from 0.005° to 0.00025° (**Supplementary Figure 7**). For pixels undergoing deforestation, we applied the relative loss of soil organic carbon after land-use change adopted from refs. [19,174], according to the forest loss driver [16] and forest successional stage [86] (**Supplementary Table 4**). The uncertainty was estimated based on the map of the interquartile range of soil carbon stocks [173]. $E_{D,peat}$ was calculated by applying an emission factor from the IPPC Wetland Report [175] to the annual forest loss data from GFW [74,75] and TMF [56] in peatlands (defined following GFW) [176–178]. The uncertainty was based on the reported uncertainty of the emission factors.

Net aquatic carbon flux ($F_{aquatic}$)

We quantified the net carbon flux in aquatic ecosystems ($F_{aquatic}$) by summing carbon removals due to organic carbon exported by rivers to oceans (F_{rivers}), carbon buried in inland water sediment (F_{burial}), and carbon sequestration by coastal vegetation ($F_{\text{coastal vegetation}}$) (**Supplementary Figure 6**), with the uncertainty calculated using error propagation.

$$F_{aquatic} = F_{rivers} + F_{burial} + F_{\text{coastal vegetation}} \quad \textbf{(Equation 5)}$$

First, we quantified F_{rivers} by estimating the Monte Carlo median and interquartile range from three refs. [76,78,79] only considering particulate (POC) and dissolved (DOC) organic carbon fluxes. Second, we quantified carbon burial in sediment of lakes and reservoirs using the average flux for lakes and reservoirs [69] per basin (uncertainty equaling 60% of estimate [55]) combined with the area of lakes and reservoirs from the Global Lakes and Wetlands Database (GLWD) version 2 [68]. Additionally, we calculated carbon burial on floodplains using the area-weighted global estimate from Regnier et al. [77] and country-level floodplain extents from GLWD version 2 [68]. Third, to compute $F_{coastal\ vegetation}$, we summed national-scale carbon fluxes in mangroves [179], salt marshes [73], and seagrasses [72,180] by multiplying country-level surface areas by area-weighted median flux rates at the African continental or global level from Rosentreter et al. [71], with the uncertainty equaling the interquartile range.

Carbon dioxide outgassed from rivers, lakes, reservoirs, and estuaries was initially assimilated by the vegetation, but was subsequently not stored in biomass and soil carbon stocks due to being leached or eroded to adjacent waters [77,181]. Therefore, following the mass balance principle, we assumed that initial removals (not included in ΔC_{intact}) completely compensated carbon emissions from inland and estuarine waters (i.e., net flux equaling zero) (**Supplementary Figure 6**).

Lateral carbon fluxes due to trade in crop and wood products ($F_{crop+wood}$)

The carbon import and export fluxes related to trade of crop and wood product ($F_{crop+wood}$) were taken from Byrne et al. [67] ($F_{crop+wood}$), with an uncertainty equaling 30% of the national estimate [67].

Top-down national net ecosystem exchange

Top-down atmospheric inversions quantify net land carbon fluxes by modeling atmospheric CO_2 transportation. To quantify the top-down NEE, we used the ensemble of 14 atmospheric inversion models from the Global Carbon Budget (GCB) 2024 at resolution 1° [36,66] (**Supplementary Figure 8**). We calculated the top-down NEE by subtracting fossil fuel emissions from GCP's Gridded Fossil Emissions Dataset version 2024.0 [182] from the net carbon flux. Using a

Monte Carlo approach, we then estimated the top-down NEE based on the median of 10,000 generated Gaussian distributions (n=1,000) based on all inversions (**Figure 4**). The uncertainty equaled the median of the interquartile ranges from all generated distributions. Since lateral carbon fluxes due to rivers and trade ($\mathrm{F_{rivers}} + \mathrm{F_{crop+wood}}$) (differing from lateral river flux correction of GCB 2024; see above) were not included in the inversions, we corrected national top-down NEE for these lateral fluxes. The final uncertainty of top-down NEE was quantified based on error propagation of the interquartile ranges of the national net and lateral carbon fluxes.

To assess the robustness of the fluxes in African moist forest-rich countries estimated by the inverse models, we repeated the analysis of Gaubert et al. [29] to quantify an emergent constraint of the CO_2 flux for our region of interest (i.e., tropical Africa between 18.5°N and 17.5°S) by comparing posterior mole fractions from the inversions with independent in-situ airborne observations measured over the tropical Atlantic Ocean during the four Atmospheric Tomography (ATom) missions. We first extracted CO_2 observations and simulated mole fractions from the inversions for all four ATom flights within our region and binned the data into 500m elevational bins [36,66]. Subsequently, we selected bins with the highest correlation between inversion fluxes and observation-based mole fractions. Using these bins, we calculated monthly mean fluxes for each of the four ATom flights using linear regression of the inversion fluxes and the mole fraction difference between the inversions and observations. Then, the ensemble mean of the inversions was fitted to the observation-based fluxes. Subsequently, the standard deviation was calculated by bootstrapping the observation uncertainties from Gaubert et al. [29] and regression fit uncertainties. We found an emergent constraint of the CO_2 flux in tropical Africa equaling to 0.1 ± 0.36 PgC yr^{-1} (mean ± standard deviation (SD)). All inversions were within the 95% confidence interval (CI) (2*SD) of this observation-based constraint, but four inversions (CAMS-Satellite, IAPCAS, COLA, and NISMON-CO2) were outside of the 68% CI (SD). Ultimately, we quantified the Monte Carlo median of the NEE of the whole region using models within the range of the 68% (standard deviation) and 95% (2*standard deviation) confidence intervals (CI) of the emergent constraint of our region of interest (**Supplementary Table 3**).

Furthermore, to assess the sensitivity of the top-down NEE estimates to the prior data on fire emissions and the observation type of atmospheric CO_2 mole fractions, we calculated Monte Carlo medians of the NEE of the whole region using inversions with/without explicit fire carbon emissions as prior data, and models using atmospheric CO_2 mole fractions from satellites, ground measurements, and a combination of both (**Supplementary Table 3**).

Ensemble national net ecosystem exchange

Using the median (assumed to equal mean) and the interquartile range (converted to standard deviation by dividing by 1.35) of the top-down and bottom-up NEE, we quantified the median national-level net ecosystem exchanges following a Monte Carlo approach assuming a symmetric Gaussian distribution, with the interquartile range as uncertainty.

To assess whether NEEs significantly differed from zero, we generated 1,000,000 random data points from a Gaussian distribution using the region/country-specific median and interquartile range (converted to standard deviation by dividing by 1.35). P-values were determined by quantifying the percentage of data with an opposite sign to the reported median NEE. By subtracting P-value from 100%, we estimated the certainty of the direction of the NEE per region. Additionally, to statistically compare bottom-up and top-down NEE estimates, we estimated p-values by calculating the percentage of data within the 95% confidence interval of each approach per region.

Quantifying net ecosystem exchange using alternative bottom-up approaches

To validate our bottom-up and top-down estimates, we calculated the NEE using four other bottom-up approaches (**Supplementary Figure 11**). First, we extracted national-level NEE from land use, land-use change, and forestry (LULUCF) from Grassi et al. [125], which was calculated using gap-filled carbon fluxes based on UNFCCC reports. We corrected for lateral carbon fluxes ($\mathrm{F_{crop+wood}} + \mathrm{F_{rivers}}$; see above) and carbon burial in sediment ($\mathrm{F_{burial}}$; see above).

Second, we quantified the NEE by calculating total changes in aboveground biomass carbon stocks using Soil Moisture and Ocean Salinity (SMOS) L-VOD data [30,34], accounting for lateral and

burial carbon fluxes (see above). Soil, deadwood, litter, and belowground biomass carbon stock changes were excluded due to high uncertainty [55].

Third, we estimated national-scale net carbon fluxes of terrestrial ecosystems (i.e., gross primary productivity minus ecosystem respiration) using the flux tower data-driven global map X-BASE [126]. Since this only included carbon removals in structurally intact terrestrial ecosystems, we accounted for carbon emissions related to CO_2 outgassing in inland and coastal waters (F_{outgas}; described below), land-use change emissions (F_{LUC}; see above), and emissions from biogenic volatile organic compounds (BVOCs) [183] to calculate NEE. We excluded carbon emissions related to wood and crop products, and geological processes [181]. We quantified total carbon emissions due to aquatic CO_2 evasion (F_{outgas}) by summing carbon fluxes in inland waters ($F_{rivers+lakes+reservoirs\ outgas}$; rivers, lakes, and reservoirs), coastal waters ($F_{estuaries}$), and coastal vegetation ($F_{coastal\ vegetation}$; see above) (**Supplementary Figure 6**). We first used the carbon efflux rate map from Liu et al. [184] to estimate CO_2 outgassing in rivers. Second, we calculated carbon emissions in lakes and reservoirs by using regional carbon efflux rates from Raymond et al. [185]. The uncertainty equaled 50% of the national-level estimate [55]. Third, to compute $F_{estuaries}$, we summed national-scale carbon fluxes in tidal systems/deltas and lagoons [70] by multiplying country-level surface areas by area-weighted median flux rates at the African continental or global level from Rosentreter et al. [71], with the uncertainty equaling the interquartile range. The final estimate of F_{outgas} equaled the sum of the carbon fluxes in inland and coastal waters, with the uncertainty calculated using error propagation.

Carbon emission through fossil fuel combustion (F_{Fo})

Carbon emissions through fossil fuel combustion, oxidation and cement production (F_{Fo}) were quantified using the global compilation of national data reported by the Global Carbon Budget [26]. Bunker fuel emissions were excluded. The uncertainty equaled 5% of the emissions [26]. Then, to highlight the relevance of preserving the net carbon sinks in African tropical moist forest-rich countries, we compared bottom-up and top-down NEE with fossil fuel emissions at a national and regional level (**Table 1**).

References

1. Hubau, W. *et al.* Asynchronous carbon sink saturation in African and Amazonian tropical forests. *Nature* **579**, 80–87 (2020).
2. Céline, E. *et al.* National forest cover change in Congo Basin: Deforestation, reforestation, degradation and regeneration for the years 1990, 2000 and 2005. *Global Change Biology* **19**, 1173–1187 (2013).
3. White, L. J. T. *et al.* Congo Basin rainforest - invest US$150 million in science. *Nature* **598**, 411–414 (2021).
4. Ciais, P. C. *et al.* The carbon balance of Africa: Synthesis of recent research studies. *Philosophical Transactions of the Royal Society A: Mathematical, Physical and Engineering Sciences* **369**, 2038–2057 (2011).
5. Valentini, R. *et al.* A full greenhouse gases budget of africa: Synthesis, uncertainties, and vulnerabilities. *Biogeosciences* **11**, 381–407 (2014).
6. Van Der Werf, G. R. *et al.* Global fire emissions and the contribution of deforestation, savanna, forest, agricultural, and peat fires (1997-2009). *Atmospheric Chemistry and Physics* **10**, 11707–11735 (2010).
7. Avitabile, V. *et al.* An integrated pan-tropical biomass map using multiple reference datasets. *Global Change Biology* **22**, 1406–1420 (2016).
8. Baccini, A. *et al.* Estimated carbon dioxide emissions from tropical deforestation improved by carbon-density maps. *Nature Climate Change* **2**, 182–185 (2012).
9. Saatchi, S. S. *et al.* Benchmark map of forest carbon stocks in tropical regions across three continents. *Proceedings of the National Academy of Sciences of the United States of America* **108**, 9899–9904 (2011).

10. Baccini, A. *et al.* Tropical forests are a net carbon source based on aboveground measurements of gain and loss. *Science* **358**, 230–234 (2017).

11. Fisher, J. B. *et al.* African tropical rainforest net carbon dioxide fluxes in the twentieth century. *Philosophical Transactions of the Royal Society B: Biological Sciences* **368**, 13–17 (2013).

12. Ellis, P. W. *et al.* The principles of natural climate solutions. *Nature Communications* **15**, (2024).

13. Girardin, C. A. J. *et al.* Nature-based solutions can help cool the planet-if we act now. *Nature* **593**, (2021).

14. Lewis, S. L., Wheeler, C. E., Mitchard, E. T. A. & Koch, A. Regenerate natural forests to store carbon. *Nature* **568**, 25–28 (2019).

15. Mo, L. *et al.* Integrated global assessment of the natural forest carbon potential. *Nature* https://doi.org/10.1038/s41586-023-06723-z (2023) doi:10.1038/s41586-023-06723-z.

16. Curtis, P. G., Slay, C. M., Harris, N. L., Tyukavina, A. & Hansen, M. C. Classifying drivers of global forest loss. *Science* **361**, 1108–1111 (2018).

17. Megevand, C. *et al.* Deforestation Trends in the Congo Basin. *Agriculture* https://doi.org/10.1596/978-0-8213-9742-8 (2013) doi:10.1596/978-0-8213-9742-8.

18. Tyukavina, A. *et al.* Congo Basin forest loss dominated by increasing smallholder clearing. *Science Advances* **4**, (2018).

19. Feng, Y. *et al.* Doubling of annual forest carbon loss over the tropics during the early twenty-first century. *Nature Sustainability* **5**, 444–451 (2022).

20. Liu, J. *et al.* Contrasting carbon cycle responses of the tropical continents to the 2015–2016 El Niño. *Science* **358**, (2017).

21. Pan, Y. *et al.* The enduring world forest carbon sink. *Nature* **631**, 563–569 (2024).

22. Gomez, D. & Irving, W. 2019 REFINEMENT TO THE 2006 IPCC GUIDELINES FOR NATIONAL GREENHOUSE GAS INVENTORIES. 1–15 (2019).

23. Jia, G. *et al. Chapter 2 Land-Climate Interactions : An IPCC Special Report on Climate Change, Desertification, Land Degradation, Sustainable Land Management, Food Security, and Greenhouse Gas Fluxes in Terrestrial Ecosystems*. 131–247 (2019).

24. Bombelli, A. *et al.* An outlook on the Sub-Saharan Africa carbon balance. *Biogeosciences* **6**, (2009).

25. Ciais, P., Piao, S.-L., Cadule, P., Friedlingstein, P. & Chédin, A. *Variability and Recent Trends in the African Terrestrial Carbon Balance*. *Biogeosciences* vol. 6 www.biogeosciences.net/6/1935/2009/ (2009).

26. Friedlingstein, P. *et al.* Global Carbon Budget 2023. *Earth System Science Data* **15**, 5301–5369 (2023).

27. Kondo, M. *et al.* State of the science in reconciling top-down and bottom-up approaches for terrestrial CO2 budget. *Global Change Biology* **26**, 1068–1084 (2020).

28. Ernst, Y. *et al.* The African Regional Greenhouse Gases Budget (2010–2019). *Global Biogeochemical Cycles* **38**, (2024).

29. Gaubert, B. *et al.* Neutral Tropical African CO2 Exchange Estimated From Aircraft and Satellite Observations. *Global Biogeochemical Cycles* **37**, (2023).

30. Zhao, Z. *et al.* Central African biomass carbon losses and gains during 2010–2019. *One Earth* **7**, 506–519 (2024).

31. Harris, N. L. *et al.* Global maps of twenty-first century forest carbon fluxes. *Nature Climate Change* **11**, 234–240 (2021).

32. Xu, L. *et al.* Changes in global terrestrial live biomass over the 21st century. *Sci. Adv* **7**, (2021).

33. Wigneron, J.-P. *et al.* Tropical forests did not recover from the strong 2015–2016 El Niño event. *Science Advances* **6**, eaay4603 (2020).

34. Yang, H. *et al.* Global increase in biomass carbon stock dominated by growth of northern young forests over past decade. *Nature Geoscience* https://doi.org/10.1038/s41561-023-01274-4 (2023) doi:10.1038/s41561-023-01274-4.

35. Anthony Bloom, A. *et al.* Lagged effects regulate the inter-annual variability of the tropical carbon balance. *Biogeosciences* **17**, 6393–6422 (2020).

36. Friedlingstein, P. *et al.* Global Carbon Budget 2024. *Earth System Science Data* **17**, 965–1039 (2025).

37. Ke, P. *et al.* Low latency carbon budget analysis reveals a large decline of the land carbon sink in 2023. *National Science Review* **11**, (2024).

38. Sitch, S. *et al.* Evaluation of the terrestrial carbon cycle, future plant geography and climate-carbon cycle feedbacks using five Dynamic Global Vegetation Models (DGVMs). *Global Change Biology* **14**, 2015–2039 (2008).

39. Brandt, M. *et al.* Satellite-Observed Major Greening and Biomass Increase in South China Karst During Recent Decade. *Earth's Future* https://agupubs.onlinelibrary.wiley.com/doi/full/10.1029/2018EF000890 (2018).

40. McNicol, I. M., Ryan, C. M. & Mitchard, E. T. A. Carbon losses from deforestation and widespread degradation offset by extensive growth in African woodlands. *Nature Communications* **9**, (2018).

41. Santoro, M. & Cartus, O. ESA Biomass Climate Change Initiative (Biomass_cci): Global datasets of forest above-ground biomass for the years 2010, 2015, 2016, 2017, 2018, 2019, 2020 and 2021, v5.01. *NERC EDS Centre for Environmental Data Analysis* https://dx.doi.org/10.5285/bf535053562141c6bb7ad831f5998d77 (2024) doi:10.5285/bf535053562141c6bb7ad831f5998d77.

42. Rodríguez-Veiga, P., Wheeler, J., Louis, V., Tansey, K. & Balzter, H. Quantifying Forest Biomass Carbon Stocks From Space. *Curr Forestry Rep* **3**, 1–18 (2017).

43. Wang, M. *et al.* A consistent record of vegetation optical depth retrieved from the AMSR-E and AMSR2 X-band observations. *International Journal of Applied Earth Observation and Geoinformation* **105**, 102609 (2021).

44. Bennett, A. C. *et al.* Resistance of African tropical forests to an extreme climate anomaly. *PNAS* **118**, (2021).

45. Carle, H. *et al.* Aboveground biomass in Australian tropical forests now a net carbon source. *Nature* **646**, 611–618 (2025).

46. ForestPlots.net *et al.* Taking the pulse of Earth's tropical forests using networks of highly distributed plots. *Biological Conservation* **260**, 108849 (2021).

47. Koch, A., Hubau, W. & Lewis, S. L. Earth System Models Are Not Capturing Present-Day Tropical Forest Carbon Dynamics. *Earth's Future* **9**, (2021).

48. Lewis, S. L. *et al.* Increasing carbon storage in intact African tropical forests. *Nature* **457**, 1003–1006 (2009).

49. Phillips, O. L. & Lewis, S. L. Evaluating the tropical forest carbon sink. *Global Change Biology* **20**, 2039–2041 (2014).

50. Mostefaoui, M. *et al.* Greenhouse gas emissions and their trends over the last 3 decades across Africa. *Earth System Science Data* **16**, 245–275 (2024).

51. Tubiello, F. N. *et al.* Carbon emissions and removals from forests: New estimates, 1990-2020. *Earth System Science Data* **13**, 1681–1691 (2021).

52. Palmer, P. I. *et al.* Net carbon emissions from African biosphere dominate pan-tropical atmospheric CO2 signal. *Nature Communications* **10**, 1–9 (2019).

53. Williams, C. A. *et al.* Africa and the global carbon cycle. *Carbon Balance and Management* **2**, (2007).

54. Laurance, W. F., Alonso, A., Lee, M. & Campbell, P. Challenges for forest conservation in Gabon, Central Africa. *Futures* **38**, 454–470 (2006).

55. Ciais, P. *et al.* Empirical estimates of regional carbon budgets imply reduced global soil heterotrophic respiration. *National Science Review* **8**, (2021).

56. Vancutsem, C. *et al. Long-Term (1990-2019) Monitoring of Forest Cover Changes in the Humid Tropics*. *Sci. Adv* vol. 7 https://www.science.org (2021).

57. Bloom, A. A., Exbrayat, J. F., Van Der Velde, I. R., Feng, L. & Williams, M. The decadal state of the terrestrial carbon cycle: Global retrievals of terrestrial carbon allocation, pools, and residence times. *Proceedings of the National Academy of Sciences of the United States of America* **113**, 1285–1290 (2016).

58. Seiler, C. *et al.* Are Terrestrial Biosphere Models Fit for Simulating the Global Land Carbon Sink? *Journal of Advances in Modeling Earth Systems* **14**, (2022).

59. Sitch, S. *et al.* Recent trends and drivers of regional sources and sinks of carbon dioxide. *Biogeosciences* **12**, 653–679 (2015).

60. Buendia, E. & et al. 2019 Refinement to the 2006 IPCC Guidelines for National Greenhouse Gas Inventories. in *IPCC* vol. 4 (2019).

61. Gasser, T. *et al.* The compact Earth system model OSCAR v2.2: Description and first results. *Geoscientific Model Development* **10**, 271–319 (2017).

62. Hartung, K. *et al.* Bookkeeping estimates of the net land-use change flux - A sensitivity study with the CMIP6 land-use dataset. *Earth System Dynamics* **12**, 763–782 (2021).

63. Houghton, R. A. & Castanho, A. Annual emissions of carbon from land use, land-use change, and forestry from 1850 to 2020. *Earth System Science Data* **15**, 2025–2054 (2023).

64. Cook-Patton, S. C. *et al.* Mapping carbon accumulation potential from global natural forest regrowth. *Nature* **585**, 545–550 (2020).

65. Heinrich, V. H. A. *et al.* The carbon sink of secondary and degraded humid tropical forests. *Nature* **615**, 436–442 (2023).

66. Luijkx, I. T. *et al. Global CO2 Gridded Flux Fields from 14 Atmospheric Inversions in GCB2024*. 10.18160/4R5W-VNBV (2024) doi:10.18160/4R5W-VNBV.

67. Byrne, B. *et al.* National CO2 budgets (2015-2020) inferred from atmospheric CO2 observations in support of the global stocktake. *Earth System Science Data* **15**, 963–1004 (2023).

68. Lehner, B. *et al.* Mapping the world's inland surface waters: an update to the Global Lakes and Wetlands Database (GLWD v2). (2024) doi:10.5194/essd-2024-204.

69. Mendonça, R. *et al.* Organic carbon burial in global lakes and reservoirs. *Nature Communications* **8**, (2017).

70. Laruelle, G. G., Rosentreter, J. A. & Regnier, P. Extrapolation-Based Regionalized Re-evaluation of the Global Estuarine Surface Area. *Estuaries and Coasts* **48**, 34 (2025).

71. Rosentreter, J. A. *et al.* Coastal vegetation and estuaries are collectively a greenhouse gas sink. *Nature Climate Change* **13**, 579–587 (2023).

72. UNEP-WCMC & Short FT. *Global Distribution of Seagrasses (Version 7.1). Seventh Update to the Data Layer Used in Green and Short (2003)*. (2021) doi:https://doi.org/10.34892/x6r3-d211.

73. Worthington, T. A. *et al.* The distribution of global tidal marshes from Earth observation data. *Global Ecology and Biogeography* **33**, (2024).

74. Hansen, M. C. *et al.* High-Resolution Global Maps of 21st-Century Forest Cover Change. *Science* **342**, 846–850 (2013).

75. Potapov, P. *et al.* The Global 2000-2020 Land Cover and Land Use Change Dataset Derived From the Landsat Archive: First Results. *Frontiers in Remote Sensing* **3**, (2022).

76. Liu, M. *et al.* Global riverine land-to-ocean carbon export constrained by observations and multi-model assessment. *Nature Geoscience* **17**, 896–904 (2024).

77. Regnier, P., Resplandy, L., Najjar, R. G. & Ciais, P. The land-to-ocean loops of the global carbon cycle. *Nature* **603**, 401–410 (2022).

78. Resplandy, L. *et al.* Revision of global carbon fluxes based on a reassessment of oceanic and riverine carbon transport. *Nature Geoscience* **11**, 504–509 (2018).

79. Zscheischler, J. *et al.* Reviews and syntheses: An empirical spatiotemporal description of the global surface-atmosphere carbon fluxes: Opportunities and data limitations. *Biogeosciences* **14**, 3685–3703 (2017).

80. Malhi, Y. The carbon balance of tropical forest regions, 1990-2005. *Current Opinion in Environmental Sustainability* **2**, 237–244 (2010).

81. Gumbo, D. *et al.* How have carbon stocks in central and southern Africa's miombo woodlands changed over the last 50 years? A systematic map of the evidence. *Environmental Evidence* **7**, (2018).

82. Bastos, A. *et al.* Impact of the 2015/2016 El Niño on the terrestrial carbon cycle constrained by bottom-up and top-down approaches. *Philosophical Transactions of the Royal Society B: Biological Sciences* **373**, (2018).

83. Seddon, A. W. R., Macias-Fauria, M., Long, P. R., Benz, D. & Willis, K. J. Sensitivity of global terrestrial ecosystems to climate variability. *Nature* **531**, 229–232 (2016).

84. Achard, F. *et al.* Determination of tropical deforestation rates and related carbon losses from 1990 to 2010. *Global Change Biology* **20**, 2540–2554 (2014).

85. Tegegne, Y. T., Lindner, M., Fobissie, K. & Kanninen, M. Evolution of drivers of deforestation and forest degradation in the Congo Basin forests: Exploring possible policy options to address forest loss. *Land Use Policy* **51**, 312–324 (2016).

86. Turubanova, S., Potapov, P. V., Tyukavina, A. & Hansen, M. C. Ongoing primary forest loss in Brazil, Democratic Republic of the Congo, and Indonesia. *Environmental Research Letters* **13**, (2018).

87. Friedlingstein, P. *et al.* Update on CO2 emissions. *Nature Geoscience* **3**, 811–812 (2010).

88. Houghton, R. A. & Hackler, J. L. Emissions of carbon from land use change in sub-Saharan Africa. *Journal of Geophysical Research: Biogeosciences* **111**, (2006).

89. Maxwell, S. L. *et al.* Degradation and forgone removals increase the carbon impact of intact forest loss by 626%. https://www.science.org (2019).

90. Le Quéré, C. *et al.* Trends in the sources and sinks of carbon dioxide. *Nature Geoscience* **2**, 831–836 (2009).

91. Van Der Werf, G. R. *et al. CO2 Emissions from Forest Loss*. http://tinyurl.com/kszq9t (2009).

92. Canadell, J. G., Raupach, M. R. & Houghton, R. A. Anthropogenic CO2 emissions in Africa. *Biogeosciences* **6**, 463–468 (2009).

93. Weber, U. *et al. The Interannual Variability of Africa's Ecosystem Productivity: A Multi-Model Analysis*. *Biogeosciences* vol. 6 285–295 www.biogeosciences.net/6/285/2009/ (2009).

94. Khairoun, A., Mouillot, F., Chen, W., Ciais, P. & Chuvieco, E. Global burned area datasets severely underestimate fire-related forest loss. (2022) doi:10.21203/rs.3.rs-2105969/v1.

95. Ramo, R. *et al.* African burned area and fire carbon emissions are strongly impacted by small fires undetected by coarse resolution satellite data. *Proceedings of the National Academy of Sciences of the United States of America* **118**, (2021).

96. Doetterl, S. *et al.* Aboveground vs. belowground carbon stocks in African tropical lowland rainforest: Drivers and implications. *PLoS ONE* **10**, 1–14 (2015).

97. FAO. *Global Forest Resources Assessment 2020: Main Report*. *Global Forest Resources Assessment 2020* (2020) doi:10.4060/ca9825en.

98. Sayer, E. J., Powers, J. S. & Tanner, E. V. J. Increased Litterfall in Tropical Forests Boosts the Transfer of Soil CO2 to the Atmosphere. *PLOS ONE* **2**, e1299 (2007).

99. Sayer, E. J. *et al.* Altered litter inputs modify carbon and nitrogen storage in soil organic matter in a lowland tropical forest. *Biogeochemistry* **156**, 115–130 (2021).

100. Leff, J. W. *et al.* Experimental litterfall manipulation drives large and rapid changes in soil carbon cycling in a wet tropical forest. *Global Change Biology* **18**, 2969–2979 (2012).

101. Cusack, D. F. *et al.* Decadal-scale litter manipulation alters the biochemical and physical character of tropical forest soil carbon. *Soil Biology and Biochemistry* **124**, 199–209 (2018).

102. Sayer, E. J. *et al.* Tropical forest soil carbon stocks do not increase despite 15 years of doubled litter inputs. *Sci Rep* **9**, 18030 (2019).

103. Nottingham, A. T., Meir, P., Velasquez, E. & Turner, B. L. Soil carbon loss by experimental warming in a tropical forest. *Nature* **584**, 234–237 (2020).

104. Wood, T. E. *et al.* Warming induces unexpectedly high soil respiration in a wet tropical forest. *Nat Commun* **16**, 8222 (2025).

105. Wang, H. *et al.* Land use-induced soil carbon loss in the dry tropics nearly offsets gains in northern lands. *Nature Communications* **16**, 10008 (2025).

106. Milodowski, D. T., Mitchard, E. T. A. & Williams, M. Forest loss maps from regional satellite monitoring systematically underestimate deforestation in two rapidly changing parts of the Amazon. *Environmental Research Letters* **12**, (2017).

107. Dalagnol, R. *et al.* Mapping tropical forest degradation with deep learning and Planet NICFI data. *Remote Sensing of Environment* **298**, 113798 (2023).

108. Arneth, A. *et al.* Historical carbon dioxide emissions caused by land-use changes are possibly larger than assumed. *Nature Geoscience* **10**, 79–84 (2017).

109. Bastos, A. *et al.* Sources of Uncertainty in Regional and Global Terrestrial CO2 Exchange Estimates. *Global Biogeochemical Cycles* **34**, (2020).

110. Araza, A. *et al.* Past decade above-ground biomass change comparisons from four multi-temporal global maps. *International Journal of Applied Earth Observation and Geoinformation* **118**, (2023).

111. Zhang-Zheng, H. *et al.* Contrasting carbon cycle along tropical forest aridity gradients in West Africa and Amazonia. *Nature Communications* **15**, (2024).

112. Huanyuan. Why models underestimate West African tropical forest productivity. https://doi.org/10.1101/2024.03.08.584066 doi:10.1101/2024.03.08.584066.

113. Demol, M. *et al.* Multi-scale lidar measurements suggest miombo woodlands contain substantially more carbon than thought. *Communications Earth and Environment* **5**, (2024).

114. Djiofack, B. Y. *et al.* Protecting an artificial savanna as a nature-based solution to restore carbon and biodiversity in the Democratic Republic of the Congo. *Global Change Biology* **30**, (2024).

115. Makelele, I. A. *et al.* Afrotropical secondary forests exhibit fast diversity and functional recovery, but slow compositional and carbon recovery after shifting cultivation. *Journal of Vegetation Science* **32**, (2021).

116. Ryan, C. M., Williams, M. & Grace, J. Above- and belowground carbon stocks in a miombo woodland landscape of mozambique. *Biotropica* **43**, 423–432 (2011).

117. David L. Skole, Cheikh Mbow, Maurice Mugabowindekwe, M. S. B. and J. H. S. Trees outside of forests as natural climate solutions. *Nature Climate Change* **11**, 1006–1008 (2021).

118. Heinimann, A. *et al.* A global view of shifting cultivation: Recent, current, and future extent. *PLoS ONE* **12**, (2017).

119. Sitch, S. *et al.* Trends and Drivers of Terrestrial Sources and Sinks of Carbon Dioxide: An Overview of the TRENDY Project. *Global Biogeochemical Cycles* **38**, (2024).

120. Poulter, B. *et al.* Bottom-up approaches for estimating terrestrial GHG budgets: Bookkeeping, process-based modeling, and data-driven methods. in *Balancing Greenhouse Gas Budgets:*

Accounting for Natural and Anthropogenic Flows of CO2 and other Trace Gases 59–85 (Elsevier, 2022). doi:10.1016/B978-0-12-814952-2.00010-1.

121. Lawal, S. *et al. Investigating the Response of LAI to Droughts in Southern African Vegetation Using Observations and Model-Simulations*.
122. Rogers, A. *et al.* A roadmap for improving the representation of photosynthesis in Earth system models. *New Phytologist* **213**, 22–42 (2017).
123. Exbrayat, J. F., Smallman, T. L., Bloom, A. A., Hutley, L. B. & Williams, M. Inverse Determination of the Influence of Fire on Vegetation Carbon Turnover in the Pantropics. *Global Biogeochemical Cycles* **32**, 1776–1789 (2018).
124. Sibret, T. *et al.* CongoFlux – The First Eddy Covariance Flux Tower in the Congo Basin. *Frontiers in Soil Science* **2**, (2022).
125. Grassi, G. *et al.* Harmonising the land-use flux estimates of global models and national inventories for 2000-2020. *Earth System Science Data* **15**, 1093–1114 (2023).
126. Nelson, J. A. *et al.* X-BASE: the first terrestrial carbon and water flux products from an extended data-driven scaling framework, FLUXCOM-X. (2024) doi:10.5194/egusphere-2024-165.
127. Kondo, M., Ichii, K., Takagi, H. & Sasakawa, M. Comparison of the data-driven top-down and bottom-up global terrestrial CO2 exchanges: GOSAT CO2 inversion and empirical eddy flux upscaling. *Journal of Geophysical Research: Biogeosciences* **120**, 1226–1245 (2015).
128. He, X. *et al.* Emerging multiscale insights on microbial carbon use efficiency in the land carbon cycle. *Nature Communications* **15**, 8010 (2024).
129. Upton, S. *et al.* Constraining biospheric carbon dioxide fluxes by combined top-down and bottom-up approaches. *Atmospheric Chemistry and Physics* **24**, 2555–2582 (2024).
130. Chandra, N. *et al.* Estimated regional CO2 flux and uncertainty based on an ensemble of atmospheric CO2 inversions. *Atmospheric Chemistry and Physics* **22**, 9215–9243 (2022).

131. Lauvaux, T. *et al.* Network design for mesoscale inversions of CO 2 sources and sinks. *Tellus, Series B: Chemical and Physical Meteorology* **64**, (2012).

132. Fischer, M. *et al.* Quantifying uncertainty in simulations of the West African monsoon with the use of surrogate models. *Weather and Climate Dynamics* **5**, 511–536 (2024).

133. Mutton, H. *et al.* Understanding the Uncertainty in the West African Monsoon Precipitation Response to Increasing CO2. *Journal of Climate* **38**, 3151–3168 (2025).

134. Monerie, P.-A., Dittus, A. J., Wilcox, L. J. & Turner, A. G. Uncertainty in Simulating Twentieth Century West African Precipitation Trends: The Role of Anthropogenic Aerosol Emissions. *Earth's Future* **11**, e2022EF002995 (2023).

135. de Coëtlogon, G., Deroubaix, A., Flamant, C., Menut, L. & Gaetani, M. Impact of the Guinea coast upwelling on atmospheric dynamics, precipitation and pollutant transport over southern West Africa. *Atmospheric Chemistry and Physics* **23**, 15507–15521 (2023).

136. Achugbu, I. C. *et al.* Assessment of WRF Land Surface Model Performance over West Africa. *Advances in Meteorology* **2020**, 6205308 (2020).

137. Gatti, L. V. *et al.* Amazonia as a carbon source linked to deforestation and climate change. *Nature* **595**, 388–393 (2021).

138. A network to understand the changing socio-ecology of the southern African woodlands (SEOSAW): Challenges, benefits, and methods. *Plants People Planet* **3**, 249–267 (2021).

139. Young, D. M. *et al.* Simulating carbon accumulation and loss in the central Congo peatlands. *Global Change Biology* https://doi.org/10.1111/gcb.16966 (2023) doi:10.1111/gcb.16966.

140. Chave, J. *et al.* Ground Data are Essential for Biomass Remote Sensing Missions. *Surveys in Geophysics* **40**, 863–880 (2019).

141. Barthel, M. *et al.* Low N2O and variable CH4 fluxes from tropical forest soils of the Congo Basin. *Nature Communications* **13**, 1–8 (2022).

142. Abernethy, K., Maisels, F. & White, L. J. T. Environmental Issues in Central Africa. *Annual Review of Environment and Resources* **41**, 1–33 (2016).

143. Roopsind, A., Sohngen, B. & Brandt, J. Evidence that a national REDD+ program reduces tree cover loss and carbon emissions in a high forest cover, low deforestation country. *Proceedings of the National Academy of Sciences* **116**, 24492–24499 (2019).

144. Malan, M. *et al.* Evaluating the impacts of a large-scale voluntary REDD+ project in Sierra Leone. *Nat Sustain* **7**, 120–129 (2024).

145. TFFF - Tropical Forest Forever Facility. *https://tfff.earth/* https://tfff.earth/.

146. Myers, N., Mittermeier[2], R. A., Mittermeier[2], C. G., Da Fonseca[3], G. A. B. & Kent, J. *Biodiversity Hotspots for Conservation Priorities*. *NATURE* | vol. 403 www.nature.com (2000).

147. Alkama, R. & Cescatti, A. Biophysical climate impacts of recentchanges in global forest cover. *Science* **351**, 600–604 (2016).

148. Dyer, E. L. E. *et al.* Congo Basin precipitation: Assessing seasonality, regional interactions, and sources ofmoisture. *Journal of Geophysical Research* **122**, 6882–6898 (2017).

149. Vollset, S. E. *et al.* Fertility, mortality, migration, and population scenarios for 195 countries and territories from 2017 to 2100: a forecasting analysis for the Global Burden of Disease Study. *The Lancet* **396**, 1285–1306 (2020).

150. Eba'a Atyi, R. *et al. État Des Forêts 2021. Les Forêts Du Bassin Du Congo*. (2021).

151. Ripple, W. J. *et al.* The 2024 state of the climate report: Perilous times on planet Earth. *BioScience* https://doi.org/10.1093/biosci/biae087 (2024) doi:10.1093/biosci/biae087.

152. Friedl, M. & Sulla-Menashe, D. MODIS/Terra+Aqua Land Cover Type Yearly L3 Global 500m SIN Grid V061 [Data set]. *NASA EOSDIS Land Processes Distributed Active Archive Center* https://doi.org/10.5067/MODIS/MCD12Q1.061 (2022) doi:10.5067/MODIS/MCD12Q1.061.

153. Fao. *FOOD AND AGRICULTURE ORGANIZATION OF THE UNITED NATIONS Rome*.

154. Gorelick, N. *et al.* Google Earth Engine: Planetary-scale geospatial analysis for everyone. *Remote Sensing of Environment* **202**, 18–27 (2017).

155. R Core Team. R: A Language and Environment for Statistical Computing. https://www.R-project.org/ (2020).

156. Veen, A. M. H. van der & Cox, M. G. Getting started with uncertainty evaluation using the Monte Carlo method in R. *Accreditation and Quality Assurance* **26**, 129–141 (2021).

157. Rosan, T. M. *et al.* Synthesis of the land carbon fluxes of the Amazon region between 2010 and 2020. *Communications Earth and Environment* **5**, (2024).

158. Harris, I., Osborn, T. J., Jones, P. & Lister, D. Version 4 of the CRU TS monthly high-resolution gridded multivariate climate dataset. *Sci Data* **7**, 109 (2020).

159. Fick, S. E. & Hijmans, R. J. WorldClim 2: new 1-km spatial resolution climate surfaces for global land areas. *International Journal of Climatology* **37**, 4302–4315 (2017).

160. Huffman, G. J. *et al.* The TRMM Multisatellite Precipitation Analysis (TMPA): Quasi-global, multiyear, combined-sensor precipitation estimates at fine scales. *Journal of Hydrometeorology* **8**, 38–55 (2007).

161. Zarin, D. J. *et al.* Can carbon emissions from tropical deforestation drop by 50% in 5 years? *Global Change Biology* **22**, 1336–1347 (2016).

162. Simard, M. *et al.* Mangrove canopy height globally related to precipitation, temperature and cyclone frequency. *Nature Geoscience* **12**, 40–45 (2019).

163. Bourgoin, C. *et al. Global Map of Forest Types 2020 - Version 0*. http://data.europa.eu/89h/037ca376-ba92-49db-a8f7-0c277c1e5436 (2024).

164. Obermeier, W. A. *et al.* Modelled land use and land cover change emissions-a spatio-Temporal comparison of different approaches. *Earth System Dynamics* **12**, 635–670 (2021).

165. IPCC. *Refinement to the 2006 IPCC Guidelines for National Greenhouse Gas Inventories*. vol. 6 (IGES, 2006).

166. Farr, T. G. *et al.* The shuttle radar topography mission. *Reviews of Geophysics* **45**, (2007).

167. Di Giuseppe, F., Rémy, S., Pappenberger, F. & Wetterhall, F. Using the Fire Weather Index (FWI) to improve the estimation of fire emissions from fire radiative power (FRP) observations. *Atmospheric Chemistry and Physics* **18**, 5359–5370 (2018).

168. Chen, Y. *et al.* Multi-decadal trends and variability in burned area from the fifth version of the Global Fire Emissions Database (GFED5). *Earth System Science Data* **15**, 5227–5259 (2023).

169. Potapov, P. V. *et al.* Quantifying forest cover loss in Democratic Republic of the Congo, 2000-2010, with Landsat ETM+ data. *Remote Sensing of Environment* **122**, 106–116 (2012).

170. Marín-Spiotta, E. & Sharma, S. Carbon storage in successional and plantation forest soils: a tropical analysis. *Global Ecology and Biogeography* **22**, 105–117 (2013).

171. Makelele, I. A. *et al.* Net primary productivity and carbon allocation along secondary succession in a central African tropical forest. *New Phytologist* **n/a**,.

172. Bauters, M. *et al.* Long-term recovery of the functional community assembly and carbon pools in an African tropical forest succession. *Biotropica* **51**, 319–329 (2019).

173. Poggio, L. *et al.* SoilGrids 2.0: Producing soil information for the globe with quantified spatial uncertainty. *SOIL* **7**, 217–240 (2021).

174. Don, A., Schumacher, J. & Freibauer, A. Impact of tropical land-use change on soil organic carbon stocks - a meta-analysis. *Global Change Biology* **17**, 1658–1670 (2011).

175. Hiraishi, T. *et al. 2013 Supplement to the 2006 IPCC Guidelines for National Greenhouse Gas Inventories : Wetlands : Methodological Guidance on Lands with Wet and Drained Soils, and Constructed Wetlands for Wastewater Treatment*. (2013).

176. Crezee, B. *et al.* Mapping peat thickness and carbon stocks of the central Congo Basin using field data. *Nature Geoscience* **15**, 639–644 (2022).

177. Gumbricht, T. *et al.* An expert system model for mapping tropical wetlands and peatlands reveals South America as the largest contributor. *Global Change Biology* **23**, 3581–3599 (2017).

178. Xu, J., Morris, P. J., Liu, J. & Holden, J. PEATMAP: Refining estimates of global peatland distribution based on a meta-analysis. *Catena* **160**, 134–140 (2018).

179. Bunting, P. *et al.* Global Mangrove Extent Change 1996–2020: Global Mangrove Watch Version 3.0. *Remote Sensing* **14**, (2022).

180. McKenzie, L. J. *et al.* The global distribution of seagrass meadows. *Environmental Research Letters* **15**, (2020).

181. Ciais, P. *et al.* Definitions and methods to estimate regional land carbon fluxes for the second phase of the REgional Carbon Cycle Assessment and Processes Project (RECCAP-2). https://doi.org/10.5194/gmd-2020-259 doi:10.5194/gmd-2020-259.

182. Jones, M. W. *et al.* Gridded fossil CO2 emissions and related O2 combustion consistent with national inventories 1959–2018. *Scientific Data* **8**, (2021).

183. Guenther, A. B. *et al.* The model of emissions of gases and aerosols from nature version 2.1 (MEGAN2.1): An extended and updated framework for modeling biogenic emissions. *Geoscientific Model Development* **5**, 1471–1492 (2012).

184. Liu, S. *et al.* The importance of hydrology in routing terrestrial carbon to the atmosphere via global streams and rivers. https://doi.org/10.1073/pnas.2106322119/-/DCSupplemental (2022) doi:10.1073/pnas.2106322119/-/DCSupplemental.

185. Raymond, P. A. *et al.* Global carbon dioxide emissions from inland waters. *Nature* **503**, 355–359 (2013).

186. Winkler, K. *et al.* Changes in land use and management led to a decline in Eastern Europe's terrestrial carbon sink. *Communications Earth and Environment* **4**, (2023).

Acknowledgements

We acknowledge the Global Carbon Project, which is responsible for the Global Carbon Budget and we thank the land modelling groups for producing and making available their model outputs. We thank Santiago Botía, Anthony A. Bloom, and Wouter Peters for their input on the analysis.

Funding: W.W.M.V was funded by FWO and F.R.S.-FNRS under the Excellence of Science program (EOS O.0026.22) at Ghent University. W W.H. received support from the Belgian Science Policy Office (BELSPO; projects: FED-tWIN2019-prf-075-CongoFORCE, EF/211/TREE4FLUX, B2/223/P1/DAMOCO), from the Flemish Research Council (FWO; project G014123N COBARCHIVES), and from the Belgian Directorate-General for Development Cooperation and Humanitarian Aid (DGD; projects PilotMABplus). FM was funded by the FWO as a senior postdoc and under an ERC runner-up project (FWO grants no. 1214723N and G0BHJ26N) and is thankful to this organization for its financial support. M.B. acknowledges the financial support of the European Research Council ERC Starting grant [FORECAT, grant no. 101114639]. P.R. received financial support from the European Space Agency (ESA) project Climate-space RECCAP2: Global land carbon budget and its attribution to regional drivers.

Excellence of Science program EOS O.0026.22 (WWMV)
Belgian Science Policy Office FED-tWIN2019-prf-075-CongoFORCE, EF/211/TREE4FLUX, B2/223/P1/DAMOCO (WH)
DGD PilotMABplus (WH)
ERC FORECAT 101114639 (MB)
Research Foundation Flanders 1214723N and G0BHJ26N (FM)

Author contributions: The study was designed by W.W.M.V., W.H., M.B., and S.L. Data analysis and interpretation was carried out by W.W.M.V. with support from all co-authors. Manuscript writing was carried out by W.W.M.V., M.B., and W.H. P.R. provided input and data on aquatic fluxes. P.C. and Y.F. provided SMOS-LVOD data. F.M., T.L.S., and P.C. provided input on the use of DGVMs and CARDAMOM. A.W. conducted the analysis comparing inversions with ground observations. F.J., P.I.P, I.T.L., and L.F. provided inversion data. T.L.S. provided the CARDAMOM data. J.-F. B., A.F., A.G., J.-R. M., C.E.N.E., B.A.I., A.N., and B.T. provided feedback on manuscript

writing and methodologies. Middle authors were ordered in terms of contributions. All co-authors read and approved the manuscript.

Competing interests

The authors declare no competing interests.

Code availability

Correspondence should be addressed to W.W.M.V. and W.H. Code is available on the online Zenodo repository: https://doi.org/10.5281/zenodo.18680029.

Data availability

Correspondence should be addressed to W.W.M.V. and W.H. Final national and regional carbon flux data is available on the online Zenodo repository: https://doi.org/10.5281/zenodo.18680029. Land cover data was taken from https://developers.google.com/earth-engine/datasets/catalog/MODIS_061_MCD12Q1. Country boundaries were taken from https://developers.google.com/earth-engine/datasets/catalog/FAO_GAUL_2015_level0. Forest plot measurements were taken from https://forestplots.net/data-packages/hubau-et-al-2020. Forest conversion data were taken from the Global Forest Watch (https://storage.googleapis.com/earthenginepartners-hansen/GFC-2024-v1.12/download.html and https://glad.umd.edu/dataset/GLCLUC2020) and Tropical Moist Forest (https://forobs.jrc.ec.europa.eu/TMF/data#gee). Atmospheric CO_2 concentrations were taken from the Mauna Loa record (https://gml.noaa.gov/ccgg/trends/data.html). Mean annual temperatures were taken from the Climate Research Unit CRU TS v4.07 (https://crudata.uea.ac.uk/cru/data/hrg/cru_ts_4.07/) and WorldClim version 2 (https://www.worldclim.org/). Mean monthly precipitation was taken from the Tropical Rainfall Measurement Mission (TRMM) data v7 (https://developers.google.com/earth-engine/datasets/catalog/TRMM_3B43V7) and WorldClim version 2 (https://www.worldclim.org/). Plot-level wood density estimates were taken from https://forestplots.net/data-packages/hubau-et-al-2020. Aboveground carbon density maps

were taken from five sources (**www.wageningenur.nl/grsbiomass**, https://developers.google.com/earth-engine/datasets/catalog/WHRC_biomass_tropical, https://www.pnas.org/doi/10.1073/pnas.1019576108, https://data.globalforestwatch.org/datasets/gfw::aboveground-live-woody-biomass-density/about, https://www.earthdata.nasa.gov/data/catalog/ornl-cloud-cms-global-map-mangrove-canopy-1665-1.3). Dynamic Global Vegetation Models from TRENDY v11 and CARDAMOM were downloaded from the Global Carbon Budget online repository (https://mdosullivan.github.io/GCB/). National-scale land-use change fluxes from bookkeeping models were taken from the Global Carbon Budget repository (https://globalcarbonbudget.org/the-latest-gcb-data/). Aboveground biomass recovery curves were downloaded from two source (https://zenodo.org/records/7515854#.Y8kVQEFxeUk, https://data.globalforestwatch.org/documents/2b1e75c7d6274e448954178b3bc31bea/about). Biomass carbon emissions from forest degradation from forest degradation, deforestation, and fire were taken from Xu et al. 2021 (https://zenodo.org/records/4161694). Soil carbon stocks were taken from SoilGrids version 2 (https://soilgrids.org/). The forest loss driver map was taken from Curtis et al. 2018 (https://www.globalforestwatch.org). Forest successional stages were taken from Turubanova et al. 2018 (https://glad.umd.edu/dataset/primary-forest-humid-tropics). Forest recovery trajectories were taken from two sources (https://zenodo.org/record/7515854#.Y8kVQEFxeUk and http://www.globalforestwatch.org). Peatland areas were taken from https://data.globalforestwatch.org/datasets/gfw::global-peatlands/about. Fire emissions were taken from GFAS (https://ads.atmosphere.copernicus.eu/datasets/cams-global-fire-emissions-gfas?tab=overview) and GFEDv5 (https://www.globalfiredata.org/). Organic carbon export to rivers was taken from https://figshare.com/articles/dataset/Supplementary_Data_for_Global_riverine_land-to-ocean_carbon_export_constrained_by_observations_and_multi-model_assessment/24883290 and https://meta.icos-cp.eu/objects/GpFcABoKcZMVnRUlLHRInhdM). Area of lakes and reservoirs were taken from Global Lakes and Wetlands Database (GLWD) version 2 (https://www.hydrosheds.org/products/glwd). Lateral fluxes from crop and wood products were

taken from Byrne et al. 2023 (https://ceos.org/gst/carbon-dioxide.html). Top-down inversions were taken from https://meta.icos-cp.eu/objects/GpFcABoKcZMVnRUlLHRInhdM. The X-BASE net ecosystem exchange map can be found on https://meta.icos-cp.eu/collections/zfwf1Ak2I7OlziGDTX8Xl6_T. Emissions from BVOCs can be downloaded from https://atmosphere.copernicus.eu/charts/packages/cams/. River and lake outgassing emissions were taken from https://datadryad.org/dataset/doi:10.5061/dryad.d7wm37pz9 and https://www.nature.com/articles/nature12760, respectively. Carbon fluxes in coastal ecosystems were calculated using data from https://figshare.com/articles/dataset/Coastal_GHG_data_base_Rosentreter_et_al_2023_Nature_Climate_Change/22351267?file=40454480 and https://sextant.ifremer.fr/geonetwork/srv/api/records/9e5e5d26-eea9-4729-a7bc-4f13223e0cf2. Fossil fuel emissions were taken from the Global Carbon Budget online repository (https://globalcarbonbudget.org/the-latest-gcb-data/). UNFCCC national greenhouse gas inventory data can be downloaded from https://doi.org/10.5281/zenodo.7650360. SMOS-LVOD data can be requested from Philippe Ciais and Yu Feng.

Figures

Figure 1 – Overview of bottom-up and top-down methods for calculating net ecosystem exchange. *The top-down and bottom-up approaches are shown on the left and right from the vertical dashed line, respectively. Colors represent carbon pools, including aboveground live biomass (ΔAGB; in dark green), belowground live biomass (ΔBGB; in light green), soil organic carbon (ΔSOC; in brown), deadwood and litter (ΔDWL; in light orange), and other fluxes (other; in grey). The grey box shows carbon flux components quantified using the bottom-up approach: structurally intact terrestrial ecosystems (ΔC_{intact}), land-use change (F_{LUC}), inland and coastal waters ($F_{aquatic}$: sum of lateral carbon export from river to ocean, burial in sediment, and removal in coastal vegetation), and trade in crop and wood products ($F_{crop+wood}$). The orange box shows the processes covered by each flux component, and the black box lists the used data products (see* ***Supplementary Figure 1*** *for details). Dotted lines indicate components that can represent either removals or emissions. Adapted from Winckler et al. [186].*

Figure 2 – Biomass carbon stock fluxes in structurally intact terrestrial ecosystems for 18 African tropical moist forest-rich countries, averaged from 2015 to 2019 (ΔC_{intact} ; in TgC yr-1). Negative values represent net carbon removal from the atmosphere. *Carbon removals are shown for national (left), regional (middle), and whole region (right) scales, with both median absolute (**A**) and area-weighted (**B**) values. Area refers to the total surface area of the region, excluding water bodies (from FAO [153]). Symbols represent carbon removal estimates from upscaled forest plot measurements (AfriTRON [1]; squares), Bayesian CARbon DAta–MOdel fraMework (CARDAMOM [57]; dots), and the average of 17 Dynamic Global Vegetation Models from TRENDY v11 [58,59] (DGVMs; triangles) (see legend at the bottom). Vertical lines across each symbol represent the uncertainty (standard deviation). Boxes represent the median (horizontal line) and interquartile range (box) across the three methods based on a Monte Carlo approach. Colors indicate regions: Atlantic Central Africa (green), Congo Basin (purple), West-Africa (light green). Country codes follow IBAN standards (see* ***Supplementary Table 1*** *for abbreviations).*

Figure 3 – Bottom-up estimates of carbon flux components of 18 African tropical moist forest-rich countries, averaged from 2015 to 2019. *(**A**) Absolute carbon removals (negative bars) and*

*emissions (positive bars) at national (left), regional (middle), and whole region (right) scales (in TgC yr^{-1}). Colors in the bars represent the components of median absolute carbon fluxes: carbon removal by structurally intact terrestrial ecosystems (ΔC_{intact}: from **Figure 2**), land-use change flux (F_{LUC}), net flux in aquatic ecosystems ($F_{aquatic}$: carbon exported to oceans, buried in sediment, and sequestered by coastal vegetation), and lateral carbon flux from trade in crops and wood ($F_{crop+wood}$). Countries are ranked by the magnitude (descending) and direction (source to sink) of the bottom-up net ecosystem exchange (sum of all emissions and removals), shown as a horizontal black line for each region. (**B**) Median carbon removals and emissions weighted by unit area (in MgC ha^{-1} yr^{-1}). The area refers to total surface area of the region, including water bodies (from FAO [153]). Countries are ranked by the magnitude (descending) and direction (source to sink) of the bottom-up net ecosystem exchange per hectare, shown as a horizontal black line for each region. Country codes follow IBAN standards (see **Supplementary Table 1** for abbreviations). See **Supplementary Table 2** for national-scale carbon fluxes (per hectare) with uncertainty.*

Figure 4 – Net ecosystem exchange (NEE) for 18 African tropical moist forest-rich countries, averaged from 2015 to 2019. *(**A**) Median absolute NEE (in TgC yr^{-1}) at national (left), regional (middle), and whole region (right) scales, representing the sum of removals and emissions. Symbols indicate the NEE estimates from the bottom-up (points) and top-down approach (triangles) (see legend at the bottom and **Supplementary Figure 8** for national-scale inversion model estimates). Vertical lines across each symbol represent uncertainty (interquartile range). Boxes show the ensemble NEE or median across the two methods (horizontal line) with interquartile range (box) using a Monte Carlo approach. Colors indicate regions: Atlantic Central Africa (green), Congo Basin (purple), West-Africa (light green). Countries and regions are ordered by the magnitude (descending) and direction (source to sink) of the ensemble NEE. (**B**) Area-weighted NEE (in MgC ha^{-1} yr^{-1}), with the total surface area of the region including water bodies (from the FAO [153]). Country codes follow IBAN standards (see **Supplementary Table 1** for abbreviations).*

Tables

Table 1 – Comparison of net ecosystem exchange with fossil fuel fluxes at national and regional scales for 18 African tropical moist forest-rich countries, averaged from 2015 to 2019. *Net ecosystem exchange (NEE) from bottom-up and top-down approaches, and fossil fuel emissions (F_{Fo}) are shown at both national and regional levels. Countries and regions are ordered by the magnitude of fossil fuel emissions.*

Country / Region	**F_{Fo} (in TgC yr^{-1})**	**Bottom-up NEE (in TgC yr^{-1})**	**Top-down NEE (in TgC yr^{-1})**
National			
Central African Republic (CAF)	0.1 ± 0.003	38 ± 69.2	48.8 ± 31
Guinea-Bissau (GNB)	0.1 ± 0.004	-4.7 ± 2.5	0.9 ± 1.9
Burundi (BDI)	0.1 ± 0.007	-0.2 ± 1.1	0.3 ± 1.1
Liberia (LBR)	0.2 ± 0.009	6.5 ± 5.2	-0.1 ± 2.8
Sierra Leone (SLE)	0.3 ± 0.02	6.8 ± 9.8	4.4 ± 3.7
Rwanda (RWA)	0.3 ± 0.02	0 ± 0.8	0.1 ± 0.7
Togo (TGO)	0.6 ± 0.03	-0.6 ± 2.4	3.6 ± 3.8
Guinea (GIN)	0.8 ± 0.04	5.4 ± 20	18.5 ± 16
Democratic Republic of the Congo (COD)	0.9 ± 0.04	66.8 ± 91.3	3.1 ± 151.2
Uganda (UGA)	1.4 ± 0.07	-6.1 ± 6.8	7.5 ± 7
Gabon (GAB)	1.6 ± 0.08	-14.2 ± 12.9	-12.3 ± 14.1
Republic of the Congo (COG)	1.7 ± 0.08	-10.3 ± 13.8	-14.1 ± 28.8
Equatorial Guinea (GNQ)	1.8 ± 0.09	-1 ± 1.8	-0.9 ± 0.7
Benin (BEN)	1.8 ± 0.09	0.4 ± 3.2	6.3 ± 7.5
Cameroon (CMR)	2.7 ± 0.1	-17.2 ± 14.4	2.7 ± 13.6
Ivory Coast (CIV)	3 ± 0.1	6.2 ± 11.8	9.6 ± 14.9
Ghana (GHA)	4 ± 0.2	-0.6 ± 9.7	15.2 ± 15.6
Nigeria (NGA)	31.2 ± 1.6	-17.9 ± 14.7	5.8 ± 34
Regional			
Congo Basin	2.8 ± 0.1	98.5 ± 114.7	59.8 ± 154.5

Atlantic Central Africa	7.8 ± 0.2	-42.7 ± 23.8	-24.6 ± 34.8
West-Africa	41.9 ± 1.6	1.6 ± 31.6	64.2 ± 44.5
Whole region			
Whole region	52.5 ± 1.6	57.4 ± 121.4	99.4 ± 164.5

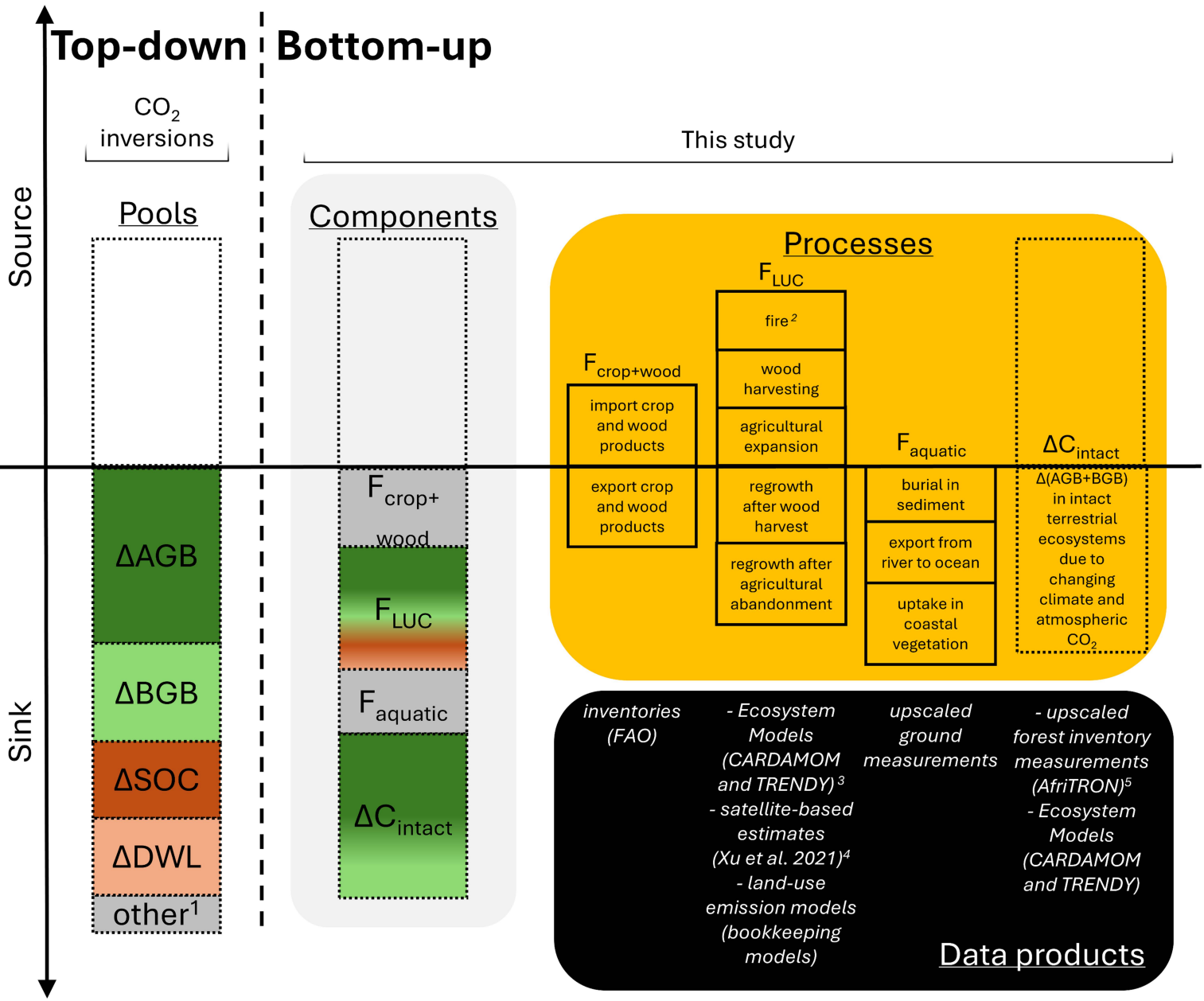

[1] inland and coastal water fluxes, geological emissions, human/animal respiration, lateral trade and river fluxes, carbon burial in sediment, crop and wood product emissions, etc.
[2] bookkeeping models do not account for fire as a management tool
[3] corrected for fire emissions using GFAS and GFEDv5
[4] no ΔSOC due to forest regrowth, and no ΔDWL
[5] only woody ecosystems
[6] lateral trade and river fluxes, and carbon burial in sediment
[7] inland and coastal water fluxes, lateral trade and river fluxes, carbon burial in sediment, and emissions from Biogenic Volatile Organic Compounds (BVOCs)

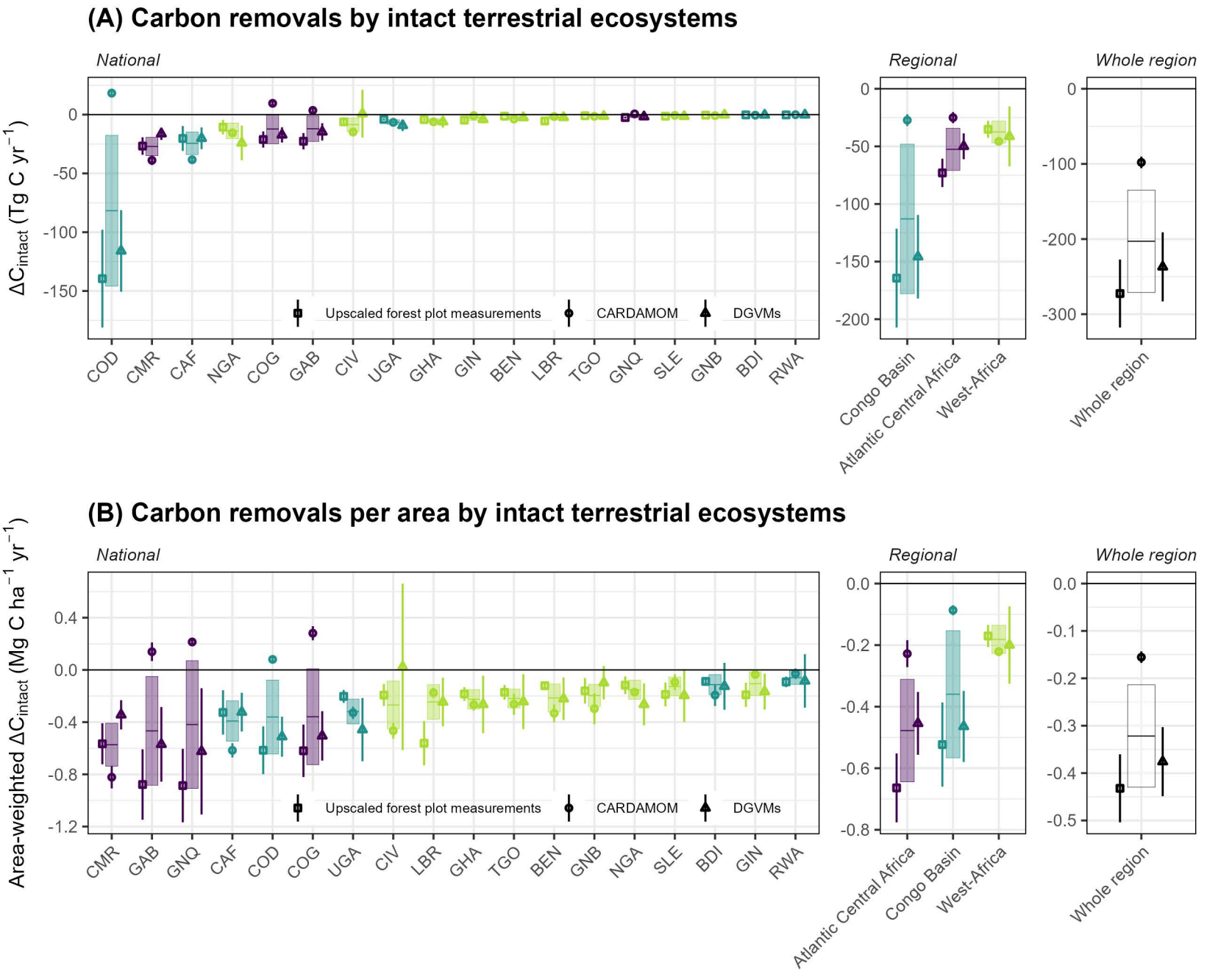
(A) Carbon removals by intact terrestrial ecosystems
National
Regional
Whole region
ΔCintact (Tg C yr−1)
Upscaled forest plot measurements
CARDAMOM
DGVMs
COD
CMR
CAF
NGA
COG
GAB
CIV
UGA
GHA
GIN
BEN
LBR
TGO
GNQ
SLE
GNB
BDI
RWA
Congo Basin
Atlantic Central Africa
West-Africa
Whole region
(B) Carbon removals per area by intact terrestrial ecosystems
Area-weighted ΔCintact (Mg C ha−1 yr−1)
CMR
GAB
GNQ
CAF
COD
COG
UGA
CIV
LBR
GHA
TGO
BEN
GNB
NGA
SLE
BDI
GIN
RWA
Atlantic Central Africa
Congo Basin
West-Africa
Whole region

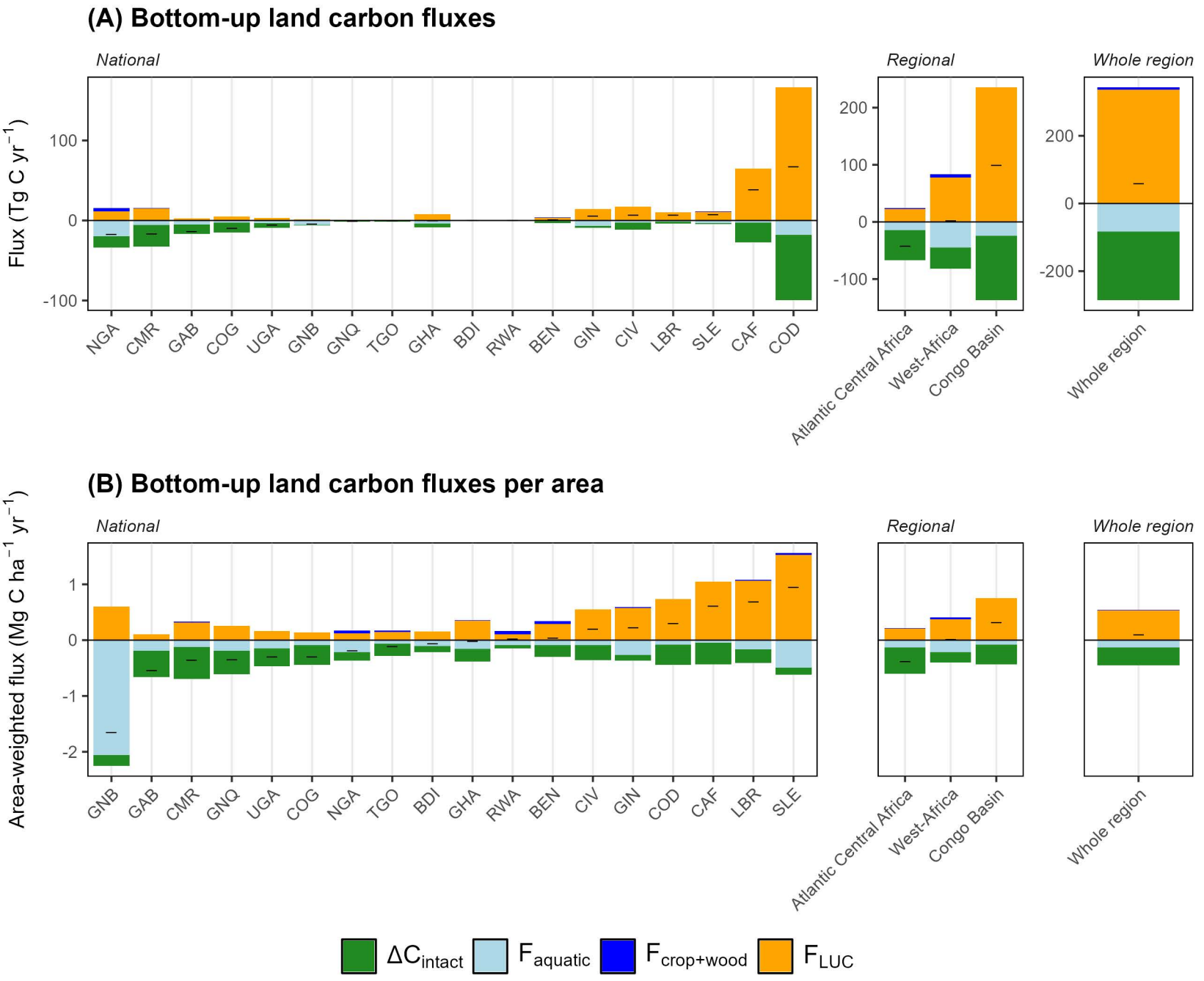
(A) Bottom-up land carbon fluxes
National
Regional
Whole region
Flux (Tg C yr^{-1})
100
0
-100
NGA
CMR
GAB
COG
UGA
GNB
GNQ
TGO
GHA
BDI
RWA
BEN
GIN
CIV
LBR
SLE
CAF
COD
200
100
0
-100
Atlantic Central Africa
West-Africa
Congo Basin
200
0
-200
Whole region
(B) Bottom-up land carbon fluxes per area
National
Regional
Whole region
Area-weighted flux (Mg C ha^{-1} yr^{-1})
1
0
-1
-2
GNB
GAB
CMR
GNQ
UGA
COG
NGA
TGO
BDI
GHA
RWA
BEN
CIV
GIN
COD
CAF
LBR
SLE
Atlantic Central Africa
West-Africa
Congo Basin
Whole region
ΔC_{intact}
$F_{aquatic}$
$F_{crop+wood}$
F_{LUC}

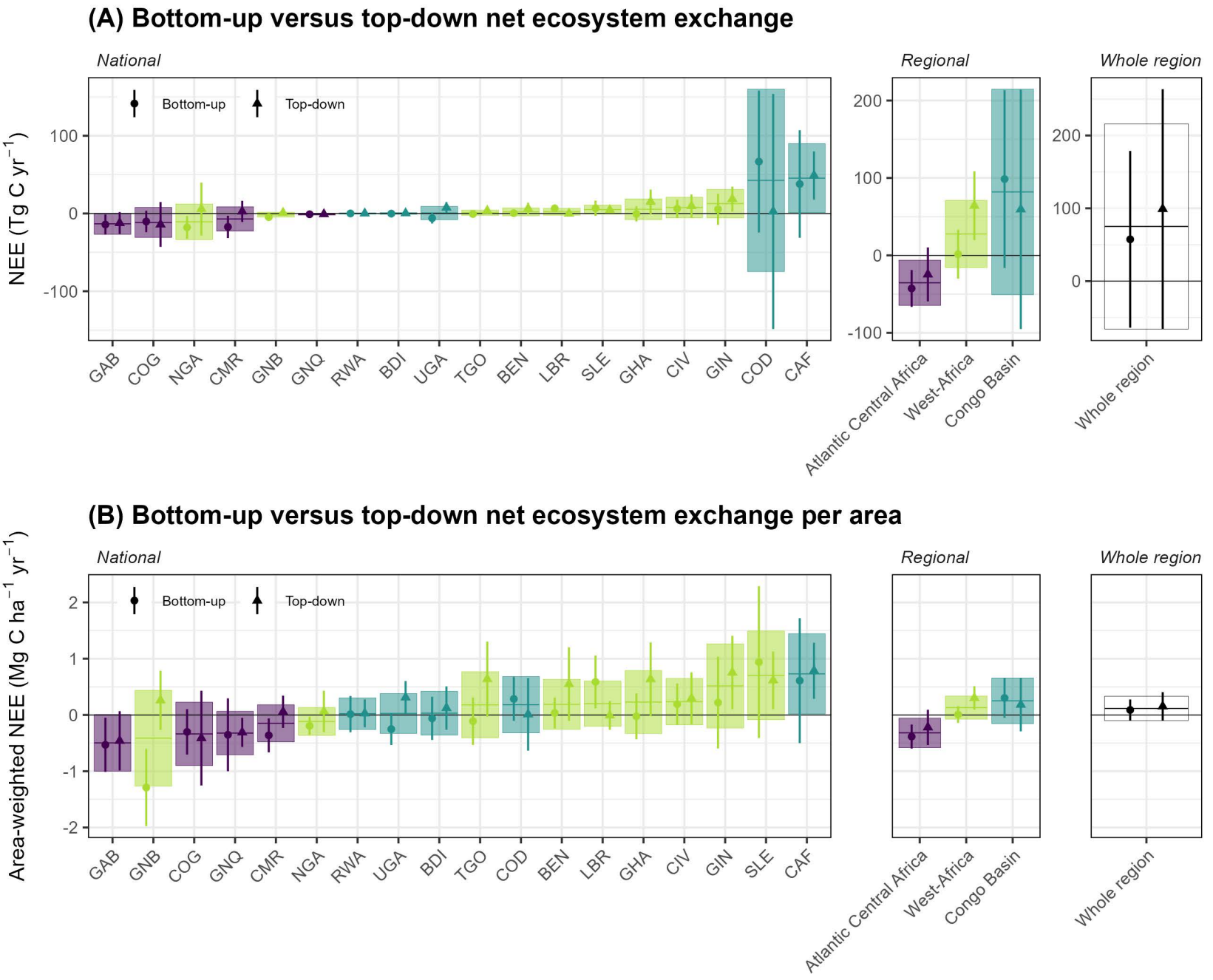
(A) Bottom-up versus top-down net ecosystem exchange
National
Regional
Whole region
Bottom-up
Top-down
NEE (Tg C yr^{-1})
100
0
-100
200
GAB
COG
NGA
CMR
GNB
GNQ
RWA
BDI
UGA
TGO
BEN
LBR
SLE
GHA
CIV
GIN
COD
CAF
Atlantic Central Africa
West-Africa
Congo Basin
Whole region
(B) Bottom-up versus top-down net ecosystem exchange per area
Area-weighted NEE (Mg C ha^{-1} yr^{-1})
2
1
0
-1
-2
GAB
GNB
COG
GNQ
CMR
NGA
RWA
UGA
BDI
TGO
COD
BEN
LBR
GHA
CIV
GIN
SLE
CAF